

Recoiling Black Hole Candidates from Spatially Offset Broad Emission Lines in MaNGA

R. SCOTT BARROWS ¹, JULIA M. COMERFORD,¹ JAMES NEGUS ², AND FRANCISCO MULLER-SANCHEZ ³

¹*Department of Astrophysical and Planetary Sciences, University of Colorado Boulder, Boulder, CO 80309, USA*

²*Cooperative Institute for Research in Environmental Sciences, University of Colorado Boulder, Boulder, CO, 80309, USA*

³*Department of Physics and Materials Science, The University of Memphis, 3720 Alumni Avenue, Memphis, TN 38152, USA*

(Accepted for publication in ApJ)

ABSTRACT

From the Mapping Nearby Galaxies at Apache Point Observatory (MaNGA) survey, we identify 14 off-nuclear broad (FWHM $> 1000 \text{ km s}^{-1}$) H α and/or H β emission line sources that indicate spatially offset active galactic nuclei (AGN) candidates. In addition to massive black holes (MBHs) in on-going galaxy mergers, this selection can also find MBHs that have been ejected from the host galaxy nucleus due to MBH binary coalescence and asymmetric gravitational wave emission or the dynamical ‘slingshot’ mechanism. Recoiling/slingshot MBHs are predicted to affect co-evolution between MBHs and their host galaxies, and they are observational tracers of past binary MBH mergers and gravitational wave emission. This is the first systematic search through an integral field spectroscopy survey for ejected MBHs to enable uniform constraints on their surface densities. We find that 42% (6/14) have optical image counterparts consistent with galaxy stellar cores from infalling MBHs before the close binary MBH stage. The remaining 58% (8/14) have large broad line luminosities relative to their stellar core mass upper limits (~ 2 times larger than for central AGN), suggesting merger-driven MBH accretion enhancements or potentially ejected MBHs. The signatures of AGN-ionized narrow emission lines for recoil/slingshot candidates are weaker by 68%, which is consistent with the ejected MBH scenario. The broad line projected velocity offsets range from $\sim 10 - 600 \text{ km s}^{-1}$ and suggest motion within the host galaxy potentials. Finally, the implied recoiling MBH surface density upper limit is consistent with predictions that assume random spin orientations in MBH binaries.

Keywords: Active galactic nuclei (16) — Emission line galaxies (459) — Galaxy mergers (608) — Gravitational waves (678) — Spectroscopy (1558) — Supermassive black holes (1663)

1. INTRODUCTION

Galaxy mergers are a potential route for co-evolution between galaxies and massive black holes (MBHs; $M_{\bullet} > 10^5 M_{\odot}$) through induced star formation, randomization of stellar orbits, and MBH growth (e.g., Di Matteo et al. 2005; Springel et al. 2005; Capelo et al. 2015). Furthermore, observations suggest that merger-driven accretion onto MBHs (visible as active galactic nuclei; AGN) may have an important role in the overall AGN population (e.g., Satyapal et al. 2014; Weston et al. 2017; Goulding et al. 2018; Gao et al. 2020).

Since galaxy mergers result in two or more MBHs that are bound to a common gravitational potential, if

the stellar cores hosting the MBHs lose sufficient angular momentum, they will eventually migrate toward the center of mass of the merger remnant. Moreover, if two MBHs form a bound binary system, they may eventually merge through the emission of gravitational waves. The final moment of coalescence will result in net gravitational wave emission that imparts a force (or recoil) on the merged MBH (e.g., Peres 1962; Bekenstein 1973) and, if strong enough, may displace it from the remnant galaxy nucleus (e.g., Campanelli et al. 2007b; Gualandris & Merritt 2008; Lousto & Zlochower 2011; for a review see Centrella et al. 2010). Alternatively, if the timescale for MBH binary coalescence is longer than the galaxy merger timescale, then a third MBH may enter the system and cause the lightest MBH to be (‘slingshot’) ejected by dynamical instabilities (e.g., Hoffman & Loeb 2007; Bonetti et al. 2016, 2018).

The recoil and slingshot phenomena will have their own unique effects on the co-evolution of galaxies and MBHs. In particular, the MBH masses that are observed to correlate with host galaxy bulge properties (e.g., Gebhardt et al. 2000; Ferrarese & Merritt 2000; Gültekin et al. 2009) will be lower due to ejection of MBHs or interrupted accretion (e.g., Volonteri 2007; Blecha et al. 2011). The distribution of recoil or slingshot velocities will also introduce scatter into those relations (e.g., Blecha & Loeb 2008; Sijacki et al. 2011). Moreover, recoiling or slingshot MBH detections will impose constraints on MBH binary formation, spin alignment, coalescence rates, and gravitational wave emission.

Practically, detection of recoiling or slingshot MBHs requires them to be actively accreting as observable AGN (see Komossa 2012 for a review of electromagnetic signatures). This scenario suggests a combination of four observables: 1) the AGN will have an unobscured broad line region (BLR; the region within which gas is gravitationally bound to the MBH and accelerated to velocities $> 1000 \text{ km s}^{-1}$ that produce Doppler broadened emission lines; e.g., Sulentic et al. 2000; Gaskell 2009); 2) if the acceleration from the recoil or slingshot is strong enough, the BLR may appear offset in velocity-space from the host galaxy systemic (e.g., Bonning et al. 2007; Komossa & Merritt 2008a; Volonteri & Madau 2008; Bogdanović et al. 2009a); 3) the BLR may have a detectable spatial offset from the host galaxy nucleus (e.g., Blecha et al. 2019); and 4) the BLR may not be spatially coincident with a detectable AGN-ionized narrow line region (NLR) if the interstellar medium (ISM) gas through which the ejected MBH travels is too diffuse or if the NLR is too small (Blecha et al. 2013). Additionally, a galaxy hosting a slingshot (rather than recoiling) MBH is more likely to also have a nuclear AGN since at least one MBH will remain in the nucleus.

Multiple systematic searches for candidate recoiling or slingshot MBHs have identified BLRs of spectroscopically classified quasi-stellar objects (QSOs) that are kinematically displaced relative to the narrow emission line systems of their host galaxies (e.g., Komossa et al. 2008b; Boroson & Lauer 2009; Bogdanović et al. 2009b; Dotti et al. 2009; Shields et al. 2009; Decarli et al. 2010; Robinson et al. 2010; Barrows et al. 2011; Steinhardt et al. 2012; Tsai et al. 2013; Markakis et al. 2015; with new sources continually discovered). However, the physical interpretation of these velocity offsets is not clear, and long-term monitoring (notably, e.g., the systematic campaign described in Eracleous et al. 2012; Runnoe et al. 2015, 2017) has revealed that most (if not all) of these kinematic BLR displacements can be explained by

accretion disk hotspots or warped accretion disks (e.g., Eracleous et al. 1995; Eracleous & Halpern 2003).

Therefore, confirmation of an off-nuclear (i.e., spatially offset) BLR is a necessary step toward finding strong recoiling or slingshot MBH candidates. Indeed, several such candidates have been identified serendipitously or from targeted follow-up spectroscopy (e.g., Koss et al. 2014; Kalfountzou et al. 2017; Chiaberge et al. 2018; Jadhav et al. 2021). However, these examples represent a small and heterogeneous collection that can not be used to understand ejected MBHs as a population.

Systematically identifying strong candidates in large numbers requires surveys with spatially-resolved spectroscopy. This requirement is currently best satisfied by the Mapping Nearby Galaxies at Apache Point Observatory (MaNGA) survey (Bundy et al. 2015), which was part of the fourth phase of the Sloan Digital Sky Survey (SDSS-IV) and is the largest integral field spectroscopy (IFS) survey to-date. Broad emission lines have previously been systematically detected in the centers of MaNGA galaxies and their companions (Steffen et al. 2022). Negus et al. (2024) recently expanded on this by using the full extent of the MaNGA IFS bundles to create a catalog of galaxies with broad emission lines detected in any spatial element (spaxel) of the MaNGA data cubes. This present work uses that catalog for the first systematic search through an IFS survey for offset BLRs to find infalling AGN in mergers and recoiling/slingshot MBH candidates.

This paper is structured as follows: in Section 2 we outline our procedure for selecting spatially offset BLR candidates, in Section 3 we describe the identification of optical image counterparts to the BLRs, in Section 4 we quantify the presence of AGN-ionized narrow emission line gas in the host galaxies, in Section 5 we discuss the possible physical nature of the offset BLRs, in Section 6 we explore the implications for merger-driven AGN triggering and detection of ejected MBHs, and in Section 7 we synthesize the results of our analysis and interpretation. Throughout we assume a flat cosmology defined by the nine-year Wilkinson Microwave Anisotropy Probe observations (Hinshaw et al. 2013): $H_0 = 69.3 \text{ km Mpc}^{-1} \text{ s}^{-1}$ and $\Omega_M = 0.287$.

2. PROCEDURE

We begin with the catalog of Negus et al. (2024) that consists of 1042 MaNGA galaxies with detected broad spectral components in at least one spaxel. The broad component identifications were based on full-width at half-maximums of $\text{FWHM} > 1000 \text{ km s}^{-1}$ associated with either of the $\text{H}\alpha$ or $\text{H}\beta$ emission lines

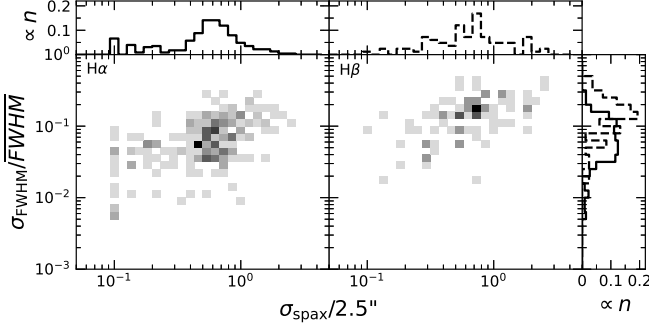


Figure 1. Linear-scale density map showing, for each galaxy, the standard deviations of the broad emission line spaxel FWHMs (normalized by the mean FWHM; $\sigma_{\text{FWHM}}/\text{FWHM}$) against the standard deviations of the spaxel spatial positions (quadrature sum of the standard deviation of the spaxels in the X- and Y-dimensions) in units of the MaNGA spatial resolution ($\sigma_{\text{spax}}/2.5$) for H α (left) and H β (right) emission line detections. Only sources with more than one broad emission line spaxel are shown. The distributions of $\sigma_{\text{FWHM}}/\text{FWHM}$ and $\sigma_{\text{spax}}/2.5$ (normalized to a sum of unity) are shown along the right and top axes, respectively, for H α (solid) and H β (dashed). The concentration of abscissa values at $\sigma_{\text{spax}}/2.5 = 0.1$ is due to sources with two adjacent broad emission line spaxels. Of the $\sigma_{\text{FWHM}}/\text{FWHM}$ values, 100% are < 1 for both H α and H β detections. Of the σ_{spax} values, 99%, 96% (H α , H β detections) are $< 2 \times 2.5$. These distributions show that the line widths and positions of the broad emission line detections in each galaxy are consistent and likely originate from a single source.

(these are the broad emission lines spectrally accessible by MaNGA) and a detection significance of $> 5\sigma$. The broad emission line components in Negus et al. (2024) were fit with a single Gaussian component (e.g., Oh et al. 2015). While AGN BLR emission may be modeled with more complex profiles (e.g., Liu et al. 2019) due to asymmetries from accretion disk hotspots or warped geometries, this choice does not alter the selection of candidate offset BLRs in this work. Therefore, we adopt these single component fits due to their uniformity for subsequent analysis and comparison.

In this work, we apply an additional threshold to the Negus et al. (2024) catalog where the broad emission line to continuum flux density ratio is > 5 times the standard deviation of the spectrum (over the fitting region), thereby accounting for the spectral quality. We have also removed cases where (assuming the host galaxy systemic redshift) multiple unidentified emission lines are observed, since this suggests the possibility that the broad emission line detections may originate from unrelated background or foreground sources. This yields 286 and 87 galaxies with H α and H β broad emission line detections in at least one spaxel, respectively, among 322 unique MaNGA galaxies. We send this sample

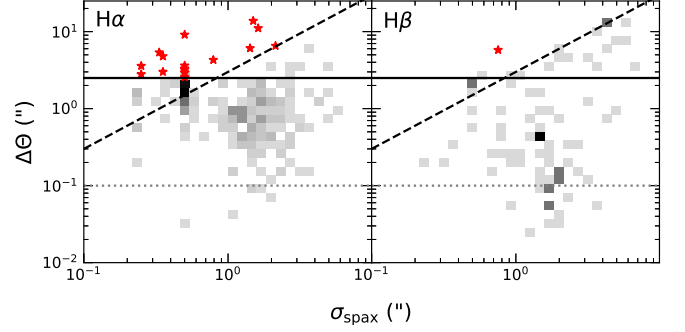


Figure 2. Angular offsets of H α (left) and H β (right) BLRs from the host galaxy centroids ($\Delta\theta$) against the source extents (σ_{spax} ; defined in Figure 1). The dotted gray line denotes the approximate MaNGA absolute astrometric uncertainty of $0''.1$. The dashed black lines denote the threshold of $\Delta\theta > 3 \times \sigma_{\text{spax}}$, and the solid black line denotes the additional uniform offset minimum of $\Delta\theta > 2''.5$ (Section 2.2). The parent sample is indicated by the linear-scale density map, while sources that pass the offset criteria are shown as red stars. The concentrations at $\sigma_{\text{spax}} = 0''.25$ and $0''.5$ are due to sources with two adjacent spaxels and those with only one spaxel (for which $\sigma_{\text{spax}} := 0''.5$, i.e., the extent of one spaxel), respectively.

through the following steps to identify spatially offset BLR candidates.

2.1. Spatial Centroids of Broad Emission Line Sources

For each galaxy, the standard deviations of the broad emission line spaxel positions (σ_{spax}) are shown in Figure 1. The values of σ_{spax} are within two times the MaNGA spatial resolution ($2''.5$) for 99%, 96% (H α , H β detections) of the sample. Therefore, at the MaNGA resolution scale, no strong evidence that the broad emission line detections are from multiple sources within each galaxy is seen. Figure 1 also shows the standard deviations of the spaxel broad emission line FWHMs (normalized by the mean FWHM: $\sigma_{\text{FWHM}}/\text{FWHM}$). All values of σ_{FWHM} are less than FWHM for H α and H β detections, thereby showing that the broad emission line widths are consistent within each galaxy.

The broad emission line detections are then assumed to originate from a single source and are referred to as BLRs. The BLR spatial centroids are taken to be the mean position of the broad emission line spaxels, weighted by the broad emission line flux. These values are computed separately for H α and H β detections.

2.2. Selection of Spatially Offset BLRs

We select BLRs from Section 2.1 with angular offsets from the centroid of the MaNGA target galaxy ($\Delta\theta$; where the target galaxy centroid comes from the SDSS pipeline and is based on the r -band image)

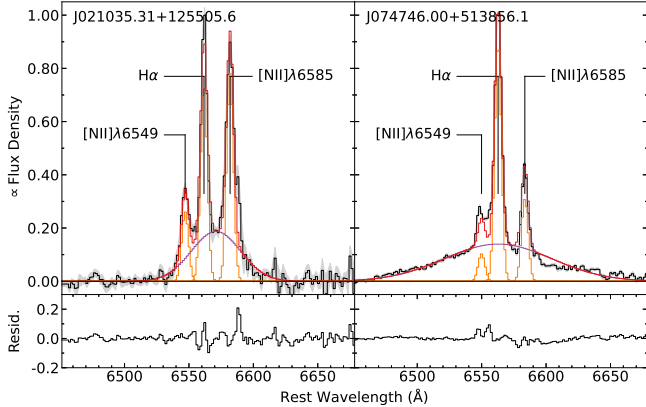


Figure 3. Best fits to the (continuum-subtracted) spectral regions (in the host galaxy rest-frame) where broad emission lines are detected. For clarity, each spectrum has been normalized by the peak flux. The narrow and broad line components are shown in orange and purple, respectively, and the model sum is shown in red. The uncertainty in the continuum subtracted spectrum is denoted by the gray-shaded region, and the residuals are shown at the bottom. Sorted by right ascension, these are the first two offset BLR sources in the sample. The remainder are shown and discussed in Section A of the Appendix (Figure 10).

by $> 3 \times \sigma_{\text{spax}}$. If a BLR has only one spaxel, then $\sigma_{\text{spax}} := 1$ spaxel. We also apply a uniform offset minimum threshold equal to the MaNGA FWHM spatial resolution ($\Delta\theta > 2''.5$) so that the sources are not contaminated by beam smearing of nuclear emission. The spatially offset selection is shown graphically in Figure 2. The MaNGA absolute astrometry is tied to that of the SDSS ($\sim 0''.1$; Law et al. 2016) and is significantly smaller than the angular offsets required by this selection, so further image registration is not necessary. This yields a sample of 14 unique spatially offset BLR candidates. One is detected in both lines, while the remaining 13 are detected only in $\text{H}\alpha$, which is consistent with $\text{H}\beta$ being the weaker of the two recombination lines. Examples of the broad emission lines are shown in Figure 3, and the remainder are shown in Section A of the Appendix. The full sample is listed in Table 1 and represents the largest compilation of spatially offset AGN that is spectroscopically selected from broad emission lines.

The BLR FWHMs (maximum value among all broad emission line spaxels in each source) and projected physical offsets of the BLR positional centroids from the host galaxy nuclei (ΔS) are listed in Table 1, and their bivariate distribution is shown in Figure 4. The FWHMs span a range that is typical of BLRs in AGN ($\text{FWHM} \approx 1000 - 5000 \text{ km s}^{-1}$), and the values of ΔS are characteristic of merging galaxy pairs ($\Delta S \approx 2 - 20 \text{ kpc}$). For comparison in our sub-

sequent analyses, central BLRs are selected to have $\Delta\theta < \sigma_{\text{spax}}$ and $\Delta\theta < 2''.5$.

3. OPTICAL IMAGE COUNTERPARTS

We use *Galfit* (Peng et al. 2010) to search for optical sources in the SDSS imaging that are spatially coincident with the BLR candidates from Section 2. Following Barrows et al. (2016, 2018), we first run *Source Extractor* (Bertin & Arnouts 1996) to obtain a list of significantly detected ($> 3\sigma$) sources. We then use these source parameters to define input Sersic components for the *Galfit* models (Sersic profiles are appropriate for fitting to the stellar bulges expected to host AGN). We also run a model that additionally has a point spread function (PSF) component to test if its inclusion improves the model based on an F -test (in no cases do we find a PSF component warrants inclusion).

We consider an SDSS image source to be associated with an offset BLR candidate if their respective spatial centroids are in agreement within $2''.5 + \sigma_{\text{spax}}$ (to be consistent with the selection of spatially offset AGN in Section 2.2). The stellar mass for each optical counterpart is estimated by applying the mass ratio between it and the host galaxy (from the *Galfit* modeling) to the host galaxy stellar mass (from *Pipe3D*; Lacerda et al. 2022; Sánchez et al. 2022). For non-detections, upper limits correspond to 5 times the local background flux. Figures 5 and 6 show galaxy images and MaNGA maps for the full samples of spatially offset $\text{H}\alpha$ and $\text{H}\beta$ BLR candidates with (6) and without (8) optical image counterpart detections, respectively. The counterpart stellar masses (or upper limits) are listed in Table 1.

The distribution of ΔS values for the subset with optical image counterparts is biased toward larger values compared to the subset without. This difference is likely due to the larger angular sizes of the MaNGA IFS hexagon bundles for the subset with image detections (mean diameter of $30''$ compared to $22''$; see Figures 5 and 6).

4. NARROW EMISSION LINE DIAGNOSTICS

To quantify the presence of extended host galaxy NLR gas that has been photo-ionized by the AGN, we examine the locations of the MaNGA spaxels on the ‘Baldwin-Phillips-Terlevich’ (or ‘BPT’) diagram. We use the calibration from Kewley et al. (2006) based on the line ratios of $[\text{O III}] \lambda 5007 / \text{H}\beta$ versus $[\text{N II}] \lambda 6585 / \text{H}\alpha$ ($[\text{N II}]$ BPT diagram) and versus $[\text{S II}] \lambda \lambda 6718, 6732 / \text{H}\alpha$ ($[\text{S II}]$ BPT diagram), where the narrow line fluxes are taken from the MaNGA Data Analysis Pipeline and are required to have signal-to-noise ratio > 3 .

Figures 5 and 6 show the locations of the spaxels within a box region of size $2 \times \sigma_{\text{spax}}$ around the BLR

Table 1. Spatially Offset Broad Emission Line Sources

Host Galaxy	z	W ($\frac{\text{km}}{\text{s}}$)	L_{BL} ($\log[\frac{\text{erg}}{\text{s}}]$)	$W_{[OIII]}$ ($\frac{\text{km}}{\text{s}}$)	$\text{Sig}_{[OIII]}$ ($-$)	ΔS (kpc)	ΔV ($\frac{\text{km}}{\text{s}}$)	$M_{*,\text{Host}}$ ($\log[M_{\odot}]$)	$M_{*,BL}$ ($\log[M_{\odot}]$)	$f_{A,BL}$	$f_{A,Nuc}$	BL	Det
($-$)	($-$)	($\frac{\text{km}}{\text{s}}$)	($\log[\frac{\text{erg}}{\text{s}}]$)	($\frac{\text{km}}{\text{s}}$)	($-$)	(kpc)	($\frac{\text{km}}{\text{s}}$)	($\log[M_{\odot}]$)	($\log[M_{\odot}]$)	$-$	$-$	($-$)	($-$)
1	2	3	4	5	6	7	8	9	10	11	12	13	14
J021035.31+125505.6	0.0996	2056 \pm 35	39.83 $^{+0.04}_{-0.04}$	373	0.1	8.9 $^{+4.7}_{-3.1}$	-292 $^{+596}_{-196}$	11.42 \pm 0.09	11.1 \pm 0.7	1.00,0.50	0.87,0.57	H α	1
J074746.00+513856.1	0.1009	4534 \pm 347	42.02 $^{+0.14}_{-0.21}$	292	2.5	20.8 $^{+5.6}_{-4.4}$	-4 $^{+103}_{-44}$	11.54 \pm 0.09	10.8 \pm 0.7	0.70,0.72	0.94,0.88	H α	1
J090401.02+012729.1	0.0534	1739 \pm 43	38.78 $^{+0.05}_{-0.06}$	256	1.0	3.5 $^{+2.7}_{-1.5}$	45 $^{+105}_{-310}$	11.02 \pm 0.09	9.7 a	0.87,0.67	0.21,0.14	H α	0
J094630.90+345500.6	0.0414	2072 \pm 49	38.84 $^{+0.05}_{-0.05}$	267	1.0	3.5 $^{+2.2}_{-1.3}$	-14 $^{+103}_{-102}$	10.99 \pm 0.06	9.2 a	0.00,0.00	0.00,0.00	H α	0
J103723.62+021845.5	0.0402	1984 \pm 112	39.31 $^{+0.11}_{-0.14}$	318	6.8	5.3 $^{+2.6}_{-1.2}$	58 $^{+105}_{-37}$	11.22 \pm 0.08	10.8 \pm 0.8	0.45,0.50	0.78,0.98	H α	1
J112458.71+470836.6	0.0537	1808 \pm 181	38.87 $^{+0.18}_{-0.30}$	299	0.2	3.0 $^{+2.7}_{-1.4}$	-28 $^{+106}_{-22}$	11.26 \pm 0.08	9.5 a	0.00,0.00	0.00,0.06	H α	0
J133938.88+272416.5	0.0351	1996 \pm 64	38.08 $^{+0.06}_{-0.08}$	349	0.2	1.8 $^{+1.8}_{-0.9}$	611 $^{+120}_{-166}$	10.97 \pm 0.07	9.1 a	0.00,0.07	0.42,0.35	H α	0
J135638.55+433508.7	0.1031	1353 \pm 36	39.35 $^{+0.05}_{-0.06}$	258	0.1	17.5 $^{+3.9}_{-2.7}$	-39 $^{+103}_{-28}$	11.36 \pm 0.09	10.9 \pm 0.7	0.00,0.00	0.00,0.01	H α	1
J150847.79+301014.0	0.0589	1562 \pm 101	38.92 $^{+0.12}_{-0.13}$	261	0.1	4.1 $^{+2.6}_{-1.7}$	-31 $^{+103}_{-27}$	11.54 \pm 0.08	9.7 a	0.00,0.00	0.00,0.00	H α	0
J160400.93+255719.4	0.0486	1010 \pm 68	38.26 $^{+0.13}_{-0.18}$	239	0.0	3.1 $^{+2.5}_{-1.4}$	-32 $^{+105}_{-25}$	11.32 \pm 0.06	9.4 a	0.00,0.00	0.00,0.00	H α	0
J161114.40+241330.0	0.0325	1347 \pm 67	37.98 $^{+0.10}_{-0.13}$	230	0.1	2.4 $^{+1.7}_{-0.9}$	-91 $^{+105}_{-49}$	10.82 \pm 0.06	9.0 a	0.00,0.00	0.00,0.00	H α	0
J163233.80+262250.6	0.0586	3620 \pm 101	39.77 $^{+0.05}_{-0.07}$	234	0.6	6.1 $^{+2.9}_{-2.0}$	50 $^{+103}_{-34}$	11.51 \pm 0.07	9.7 a	0.00,0.00	0.44,0.32	H α	0
J170450.70+344858.9	0.0564	1784 \pm 59	38.72 $^{+0.07}_{-0.08}$	253	0.9	3.3 $^{+2.9}_{-1.5}$	-11 $^{+102}_{-10}$	11.39 \pm 0.07	11.2 \pm 0.8	0.00,0.00	0.00,0.00	H α	1
J211326.02+005828.0	0.1374	4429 \pm 226	40.48 $^{+0.10}_{-0.13}$	1310	0.6	14.2 $^{+6.4}_{-4.4}$	368 $^{+1275}_{-285}$	11.66 \pm 0.08	10.9 \pm 0.8	0.00,0.00	0.21,0.04	H α , H β	1

NOTE.—Column 1: Host galaxy SDSS name; column 2: host galaxy redshift; column 3: maximum full-width at half-maximum (FWHM) of the broad emission line spaxel detections for the source; column 4: integrated broad emission line luminosity from all of the broad emission line spaxels; columns 5-6: maximum FWHM and detection significance of the outflow component (among all spaxels associated with a BLR candidate), as measured from the [O III] λ 5007 emission line; column 7: projected physical offset of the BLR positional centroid from the host galaxy centroid; column 8: projected velocity offset of the BLR (flux-weighted mean of the broad emission line spaxels) from the host galaxy systemic velocity (defined as $\Delta V = c \times (\lambda_{vac} - \lambda_{BL})/\lambda_{vac}$); column 9: stellar mass of the host galaxy; column 10: stellar mass or upper limit of the BLR optical image counterpart; columns 11-12: AGN spaxel fractions associated with the broad emission line source and the host galaxy nucleus based on the [N II], [S II] BPT diagrams; column 13: recombination line in which the BLR detection is made; and column 14: whether an SDSS image counterpart is detected (1) or not (0).

a Upper limit.

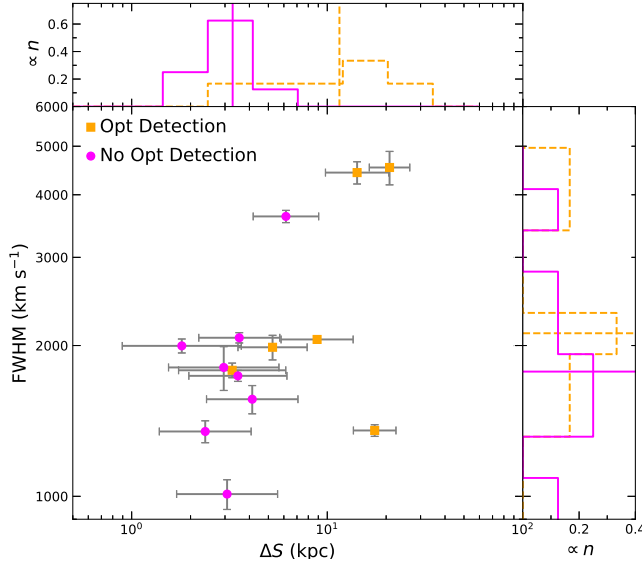


Figure 4. BLR full-width at half-maximum (FWHM; maximum value among all spaxels in each source) against projected physical offset from the host galaxy centroid (ΔS) for the final sample of spatially offset BLR candidates with (orange squares) and without (magenta circles) optical counterpart detections (Section 3). The distributions of FWHM and ΔS (each normalized to a sum of unity) are shown along the right and top axes, respectively, for the subsets with (orange, dashed) and without (magenta, solid) optical counterparts, and their median values are indicated by straight lines. The distributions of FWHM and ΔS are typical of AGN BLRs and late-stage galaxy mergers, respectively.

centroid on the [N II] and [S II] BPT diagrams. Since the MaNGA pipeline spectral fitting does not include broad components, we omit from these regions the spaxels with broad emission line detections (from [Negus et al. 2024](#)) which might affect the narrow emission line measurements. However, in our subsequent analyses, we test the effects of including these spaxels and find that the results are qualitatively unchanged (Section 5.5.1).

Following [Wylezalek et al. \(2018\)](#), we determine the fraction of these spaxels (within the box region described above) that contain ‘AGN’ emission based on the [N II] BPT diagram ($f_{A,N,BL}$) and ‘Seyfert’ or ‘LINER’ (low-ionization nuclear emission line region) emission based on the [S II] BPT diagram ($f_{A,S,BL}$). We also compute the AGN spaxel fraction centered on the nucleus of each host galaxy ($f_{A,N,Nuc}$ and $f_{A,S,Nuc}$), using the same box region as described above for uniform comparison. Values of $f_{A,BL}$ and $f_{A,Nuc}$ are listed in Table 1.

5. NATURE OF THE SPATIALLY OFFSET BLRS

In the following sections we discuss the possible nature of the spatially offset BLRs selected in this work. The discussions are presented within the context of unrelated

background or foreground sources (Section 5.1), outflows (Section 5.2), supernovae (Section 5.3), infalling MBHs in pre-coalescence mergers (Section 5.4), and re-coiling or slingshot MBHs (Section 5.5).

5.1. Background or Foreground Contaminants

Broad emission line detections in the spaxels associated with MaNGA galaxies may be emitted from background or foreground AGN and imprinted on the spectra of the galaxies. Such unrelated broad emission lines can mimic lines in the target galaxy if their observed wavelengths are near those of H α or H β in the target rest frame. Galaxies with multiple unidentified emission lines are already removed from the sample (Section 2). However, in cases where only one broad emission line is detected near the wavelengths of H α or H β in the target rest frame, the possibility of it being emitted by an unrelated source can be neither confirmed nor rejected.

To statistically quantify this possibility, we compute the number of broad emission line AGN (based on the 16th SDSS Data Release QSO catalog; [Lyke et al. 2020](#)) that would randomly be projected onto the MaNGA map for each offset AGN in our sample. The QSO redshift ranges we use are from $z=0$ to the redshift at which observed C IV $\lambda 1549$ emission from a background QSO equals that of H α in the offset BLR candidate host galaxy. Assuming any unrelated broad emission lines would be from QSOs, the highest probability of one randomly appearing within a MaNGA map from our sample is 2.7×10^{-4} .

5.2. Outflows

While the broad line selection adopted for this work echoes numerous studies finding that the threshold of 1000 km s^{-1} cleanly identifies broad line regions in H α and H β emission around AGN (e.g., [Hao et al. 2005](#); [Schneider et al. 2010](#); [Shen et al. 2011](#); [Stern & Laor 2012](#); [Oh et al. 2015](#); [Liu et al. 2019](#)), blending of multiple emission lines (i.e., in the H α /[N II] complex) that are broadened by outflows (driven by central AGN or star formation; e.g., [Wylezalek et al. 2020](#); [Meena et al. 2021](#)) can potentially mimic the presence of a single broad component in the line fitting procedure. To quantify the possibility of outflows in this work, independently of the H α complex, we test models of the continuum-subtracted [O III] $\lambda 5007$ emission line in which an additional Gaussian component is added, with an unconstrained line width intended to account for potential AGN outflows that are often seen in lines of high-ionization potential in AGN (e.g., [Komossa et al. 2008a](#)). We fit these models on the spectra of all spaxels in which broad H α components are detected.

Infalling/Pre-Coalescence BLR Candidates

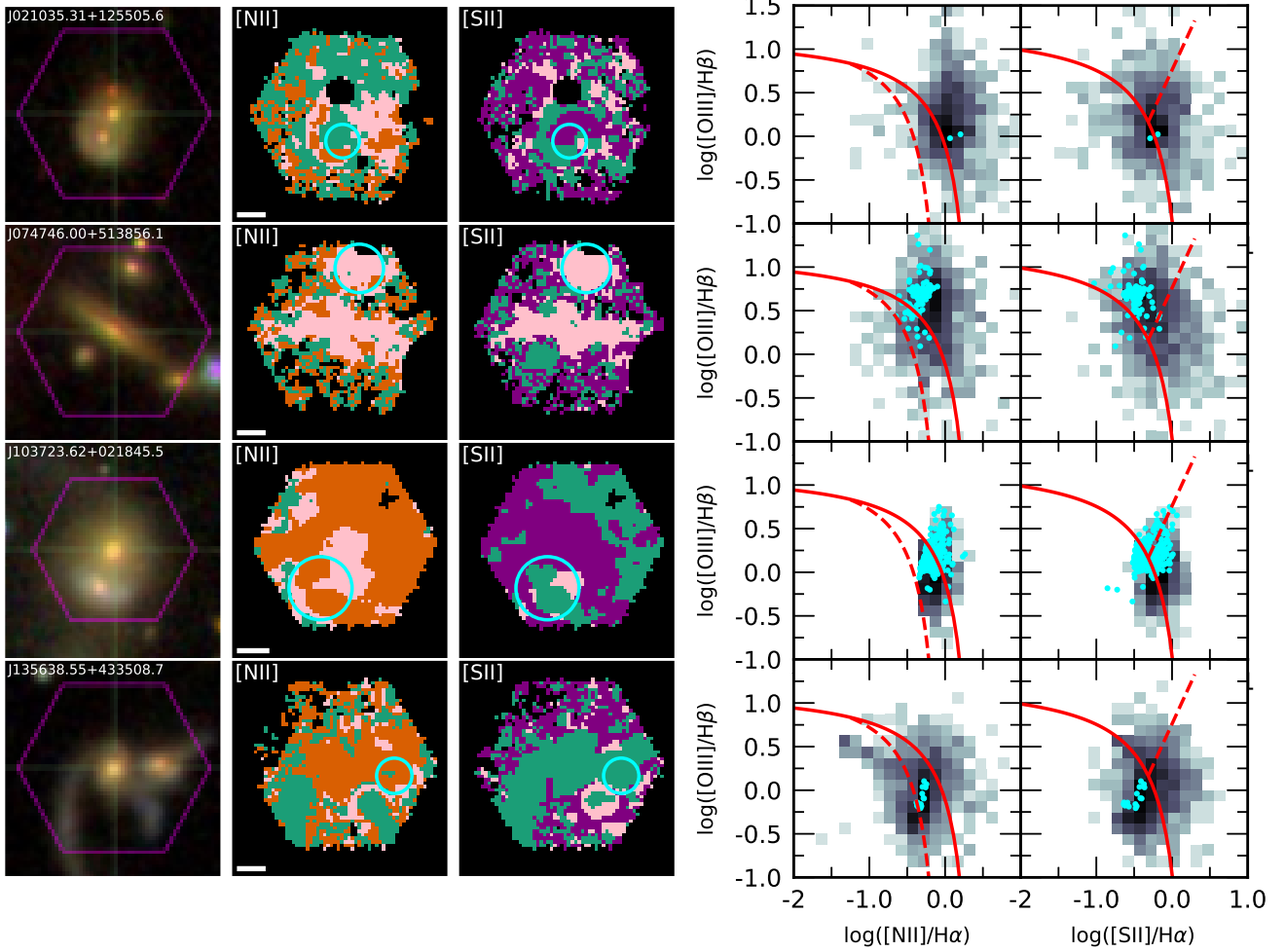


Figure 5. Full sample of MaNGA galaxies with spatially offset BLRs coincident with optical detections from the SDSS imaging. For each galaxy, the panels contain (from left to right) the SDSS $g+r+i$ color composite images (with the MaNGA IFS fiber bundle hexagon shown in magenta), the MaNGA IFS maps and BPT classifications using the [N II]-based criteria (pink = ‘AGN’, orange = ‘composite’, and green = ‘star forming’) and [S II]-based criteria (pink = ‘Seyfert’, purple = ‘LINER’, and green = ‘star forming’), and the [N II] and [S II] BPT diagrams. In the BPT plots, the solid red lines denote the pure AGN demarcation, while the dashed red lines denote the pure star formation ([N II] and LINER ([S II]) demarcations. The log-scale density map denotes spaxels from the full MaNGA map (only for spaxels with BPT classifications). The cyan dots denote the subset of the spaxels associated with the BLRs, selected to be within a box (centered on the BLR centroid) of size $2 \times \sigma_{\text{spax}}$ (to include extended narrow line region emission around the BLR) but not including the spaxels that have detected broad emission lines (since the MaNGA pipeline does not account for them). The BLR positions are indicated by the cyan circles with radii of $2''.5 + \sigma_{\text{spax}}$ (radius used for matching with optical counterparts; Section 3). The white scale bar indicates $4''$.

For each BLR candidate, the maximum FWHM value and maximum detection significance of the potential outflow components are listed in Table 1. In only one source is an additional Gaussian present at a significant ($> 3\sigma$) level (J1037), and the FWHM is 318 km s^{-1} (compared to 1984 km s^{-1} for that of the broad $H\alpha$ component). Hence, no evidence is seen for outflows that are broad enough to mimic the detected broad emission line components. This result is consistent with 13/14 of the broad emission line FWHMs in our sample exceeding the maximum outflow val-

ues observed in MaNGA galaxies ($\sim 1200 \text{ km s}^{-1}$; based on [O III] $\lambda\lambda 4959, 5008$ emission line widths; Wylezalek et al. 2020), as shown in Figure 4.

5.3. Supernovae

Hydrogren-rich supernovae (SNe) are occasionally observed to have broad Balmer emission lines with FWHMs up to several 1000 km s^{-1} (e.g., Yan et al. 2015; Kokubo et al. 2019; Kuncarayakti et al. 2023). The highly transient nature of SNe suggests that our procedure is unlikely to preferentially select them, though

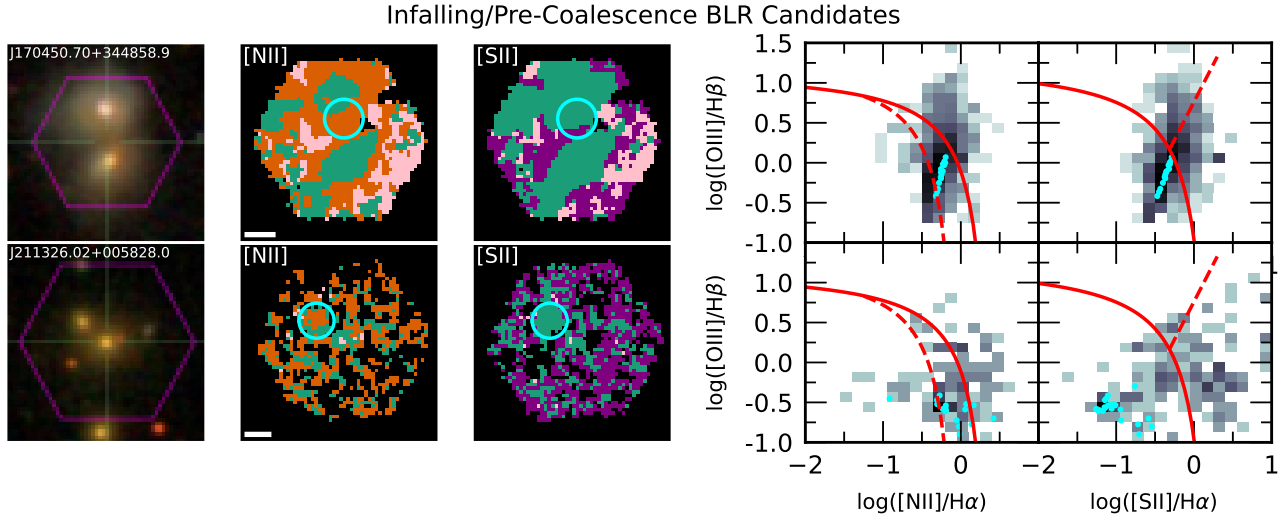


Figure 5. Continued

this possibility can not be ruled out for any individual sources. For the offset AGN candidates with optical image counterpart detections, the counterpart stellar masses strongly suggest the BLRs are associated with MBHs in galaxy nuclei, hence disfavoring the SNe explanation in these cases. However, for those without image counterpart detections (58%), the SNe possibility can not be definitively rejected with the current data. Multi-epoch spectra is the most effective means of constraining this possibility by determining whether or not the broad line emission is persistent.

5.4. Offset AGN

The masses of the hypercompact stellar systems (HCSSs; i.e., tightly gravitationally bound stellar cores) that are predicted to accompany recoiling MBHs (e.g., Guadrandis & Merritt 2008; Komossa & Merritt 2008b; Merritt et al. 2009; Li et al. 2012; Lena et al. 2020) are proportional to the MBH masses and velocity dispersions of the galaxy stellar cores where the recoils occur, and they are inversely proportional to the recoil kick velocities. Even assuming a relatively low kick velocity of 100 km s^{-1} (e.g., Schnittman & Buonanno 2007; Blecha & Loeb 2008) and a typical Milky Way bulge stellar velocity dispersion of 100 km s^{-1} (e.g., Valenti et al. 2018), the stellar masses of the 6 optical image counterpart detections in this work ($6.3 \times 10^{10} - 1.6 \times 10^{11} M_{\odot}$) are all significantly larger than their predicted HCSS masses ($\sim 10^5 - 10^7 M_{\odot}$; using the derivation from Merritt et al. 2009, assuming collisional loss cone repopulation, and using the MBH mass estimates from Negus et al. 2024). The stellar cores around slingshot MBHs will be even smaller since MBHs will remain in the host galaxy nucleus. Therefore, the offset BLR candidates with optical image counterpart detections (Figure 5) are unlikely to

be from ejected MBHs, and they are instead likely infalling (i.e., pre-coalescence) AGN in galaxy mergers or merger remnants (e.g., Müller-Sánchez et al. 2015; Barrows et al. 2017; Skipper & Browne 2018; Stemo et al. 2021; Barrows et al. 2024).

However, the 8 offset BLRs without optical image counterpart detections (Figure 6) remain recoil or slingshot candidates since, due to the absence of lower limits, their hypothetical stellar core masses are potentially consistent with values predicted for HCSSs. Indeed, using the SDSS galaxy morphological classifications of Nevin et al. (2023) and a merger probability threshold of 0.5 (i.e., Comerford et al. 2024), 37% of them are classified as post-coalescence mergers (as expected for the ejected MBH scenario).

5.5. Recoiling and Slingshot MBHs

The recoil or slingshot scenarios can be neither confirmed nor rejected with the current data for the 8 offset BLR candidates without optical image counterparts. Therefore, to further constrain the likely nature of these sources, in this section we compare the optical extended AGN-ionized emission (Section 5.5.1) and the velocity offsets (Section 5.5.2) to expectations for recoiling and slingshot MBHs.

5.5.1. Spatially Extended AGN Narrow Line Emission

If the ISM gas in the local environment of an ejected AGN is too diffuse, or if the AGN is too faint, an AGN-ionized NLR at the offset BLR position will not be detected (Blecha et al. 2013). In this scenario, sources with $f_{A,BL}$ values close to unity may be particularly weak recoil or slingshot candidates, while those with $f_{A,BL} = 0$ are the stronger candidates. Indeed, the $f_{A,BL}$ values for the offset BLRs without optical image counterparts

Recoil and Slingshot BLR Candidates

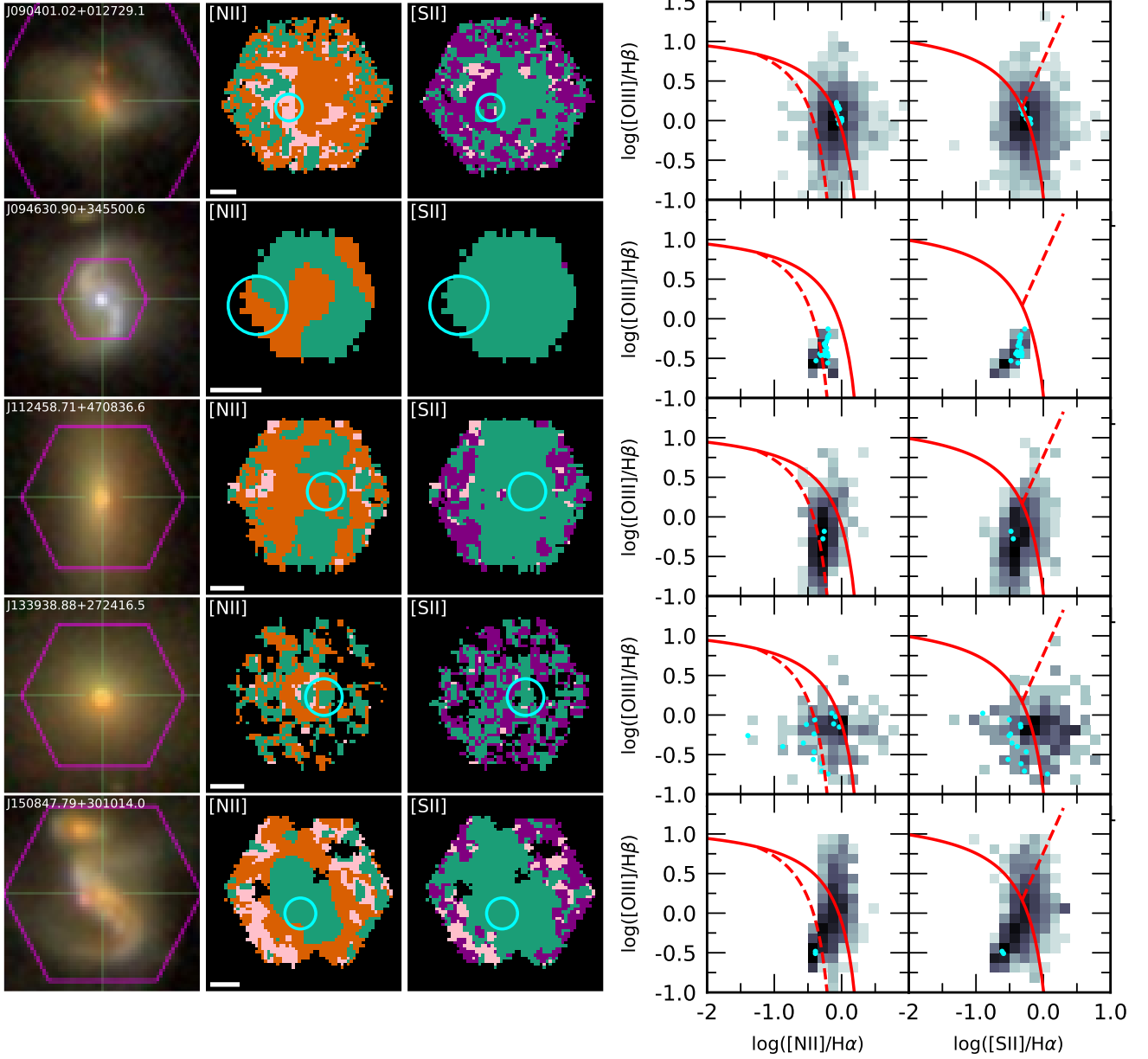


Figure 6. Same as Figure 5 but for the full sample without optical image counterpart detections.

are 70% and 68% lower (for the [N II] and [S II] diagnostics, respectively) than those with counterparts (Figure 7). Moreover, the Kolmogorov-Smirnov (KS) statistic and null hypothesis probability are 0.38 and 0.64, respectively (for both the [N II] and [S II] diagnostics), that they have similar $f_{A,BL}$ distributions. This result is qualitatively unchanged when including the spaxels with broad emission lines (see Section 4), and may provide some evidence in support of the recoil or slingshot scenarios. However, relatively low values of $f_{A,BL}$ among offset BLRs without counterparts are potentially explained by their lower AGN luminosities (the median

luminosity is 7 times smaller than for those with optical counterparts; Table 1).

AGN emission in the host galaxy nucleus may occur after a MBH slingshot if one or both of the remaining nuclear MBHs (or a coalesced MBH remnant) is actively accreting. Extended photo-ionized AGN emission may also be present in the nucleus where a recoil occurred if an AGN was previously there and its ionization signatures remain (e.g., Keel et al. 2015; LaMassa et al. 2015; Runnoe et al. 2016; Comerford et al. 2017). However, such emission is likely to have faded because the time that recoiling AGN are predicted

Recoil and Slingshot BLR Candidates

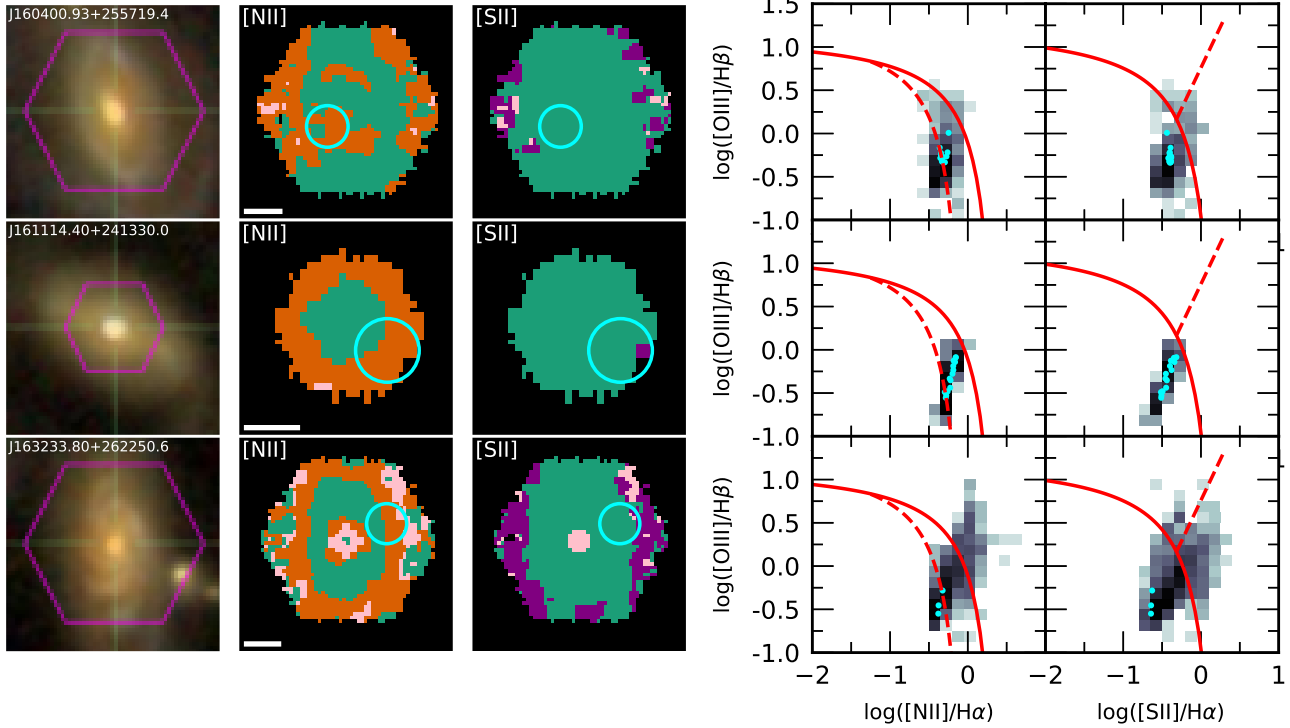


Figure 6. Continued.

to spend at the observed values of ΔS for our sample range from $\sim 1 - 10$ Myrs (Blecha et al. 2016), while light echo timescales for AGN-ionized optical emission are estimated to be only $\sim 10^4 - 10^5$ yrs for extended NLRs (e.g., Schawinski et al. 2015). Therefore, the ejected AGN candidates with $f_{A,BL} = 0$ and $f_{A,Nuc} > 0$ may be stronger slingshot candidates, while those with $f_{A,BL} = f_{A,Nuc} = 0$ may be stronger recoil candidates.

Obscuration would also attenuate NLR AGN emission in the host galaxy nuclei. However, when converting the Balmer decrements of the host galaxy nuclei into color excesses (E_{B-V} ; using the relation from Yuan et al. 2018), the host galaxy nuclei with $f_{A,Nuc} = 0$ have a mean E_{B-V} value of only 0.41, compared to the mean of 0.53 for the full sample. So there is no systematic evidence for a lack of nuclear AGN NLR emission being caused by obscuration.

5.5.2. Velocity Offsets

Theoretical work predicts that recoil (‘kick’) velocities strongly depend on the relative spin alignment of the progenitor MBHs, with relatively small kick velocities generated for more aligned MBH spins (e.g., Campanelli et al. 2007a,b; Schnittman & Buonanno 2007). The distribution of kick velocities will determine the observed distribution of recoiling MBH velocities, modulo the effects of damping due to dynamical friction (e.g., Blecha et al. 2011; Sijacki et al. 2011), oscillation within

the host galaxy (assuming the kick velocity is below the galactic escape velocity; e.g., Choksi et al. 2017), and projection onto the sky plane.

The left panel of Figure 8 shows the total BLR luminosities (L_{BL} ; integrated over all spaxels; Table 1) against the magnitudes of the BLR projected velocity offsets from the host galaxy systemic (ΔV ; flux-weighted average of the velocity offsets in the individual spaxels; Table 1). The offset AGN samples with and without optical counterparts have similar $|\Delta V|$ values (means within 10 km s^{-1} of each other) and their distributions overlap significantly with that of the central AGN. However, the offset AGN samples do show evidence for systematically larger mean $|\Delta V|$ values (by 78%). Though these values are all within the range typically expected for galaxy rotation (e.g., Sofue & Rubin 2001), this result may be indicative of motion of the spatially offset BLRs relative to the host galaxies, and the mean $|\Delta V|$ value is consistent (within 41%) with the predicted observed values for recoils in Blecha & Loeb (2008).

Furthermore, the relatively lower L_{BL} values for the offset AGN without optical image counterparts (Section 5.5.1) may be consistent with the recoil scenario in that the kick velocities are expected to reduce the AGN duty cycles since they are displaced from large reservoirs of nuclear gas and dust for accretion (Blecha et al. 2016). However, contrary to predictions that observable recoils

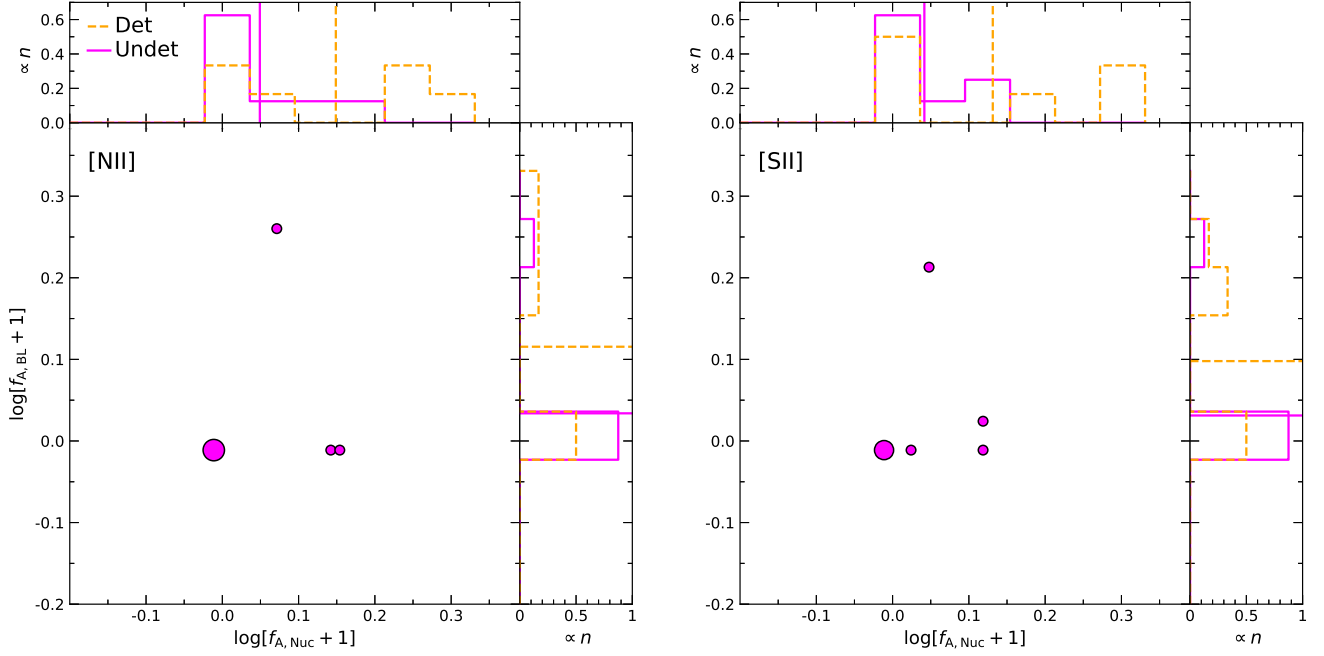


Figure 7. AGN BPT spaxel fractions of the BLRs ($f_{A,BL}$) against those of the host galaxy nuclei ($f_{A,Nuc}$) for AGN selections based on the [N II] (left) and [S II] (right) BPT diagrams for the offset AGN without optical image counterpart detections (i.e., the ejected AGN candidates; magenta circles). See Section 4 for details on the AGN spaxel fraction calculations. Since sources cluster at $f_{A,BL} = f_{A,Nuc} = 0$, marker sizes indicate the number of sources: small and large circles indicate 1 and 5 sources, respectively (left panel), and 1 and 4 sources, respectively (right panel). The distributions of $f_{A,BL}$ and $f_{A,Nuc}$ are shown along the right and top axes, respectively, normalized to a sum of unity. For comparison, the distributions for the offset AGN with optical image counterparts (i.e., likely infalling AGN; orange dashed) are also shown. The mean values are indicated with straight lines of corresponding color and style. The mean values of $f_{A,BL}$ are smallest for the ejected AGN candidates (consistent with the recoil/slingshot scenario). The mean values of $f_{A,Nuc}$ are also smaller for the ejected AGN candidates, which is more consistent with the recoil (as opposed to slingshot) scenario.

will be preferentially hosted by galaxies with low escape velocities, a bias toward lower host galaxy stellar masses is not observed.

6. RESULTS

In the following sections, we explore the implications of this offset BLR sample for the role of galaxy mergers in AGN triggering (Section 6.1), dual AGN and photoionization of the ISM on extended spatial scales (Section 6.2), and the frequency of recoiling AGN detections (Section 6.3).

6.1. Merger-Driven AGN Accretion

While galaxy mergers are effective at triggering accretion onto MBHs, whether or not this process plays a significant role in the overall AGN population is unclear. In particular, several numerical analyses suggest that the fraction of galaxies with AGN is enhanced for those in on-going mergers or merger remnants (e.g., McAlpine et al. 2020; Byrne-Mamahit et al. 2022). However, alternative results instead predict no enhancements and that the AGN luminosities are primarily regulated by the masses of their host galaxy stellar cores (e.g., Steinborn et al. 2016; Weigel et al. 2018).

The spatially constrained positions of offset AGN allow for masses or upper limits of their stellar cores to be measured, thereby facilitating tests of these predictions. Furthermore, while selection of AGN in galaxy mergers is often based on morphological signatures with clear disturbances that preferentially find major mergers (e.g., Cisternas et al. 2011; Kocevski et al. 2012; Villforth et al. 2014), the selection in this work is based on AGN signatures and is therefore also sensitive to the population of minor mergers with extreme mass ratios that dominate merger rates (e.g., Lotz et al. 2011; Duncan et al. 2019).

Figure 9 shows the relationship between L_{BL} and the stellar core mass (or upper limit) for the central AGN and the offset AGN (M_*). The overall sample does not show a bias toward relatively high L_{BL}/M_* values compared to central AGN (consistent within 1σ). If all of the offset AGN in this work (including those without optical image counterparts) are infalling AGN, this result would indicate that MBH accretion in these systems is relatively independent of the merger process. However, previous work suggests that merger-driven MBH growth may be strongest for AGN in relatively low mass galaxies (e.g., Yu et al. 2011; Capelo et al. 2015; Comerford

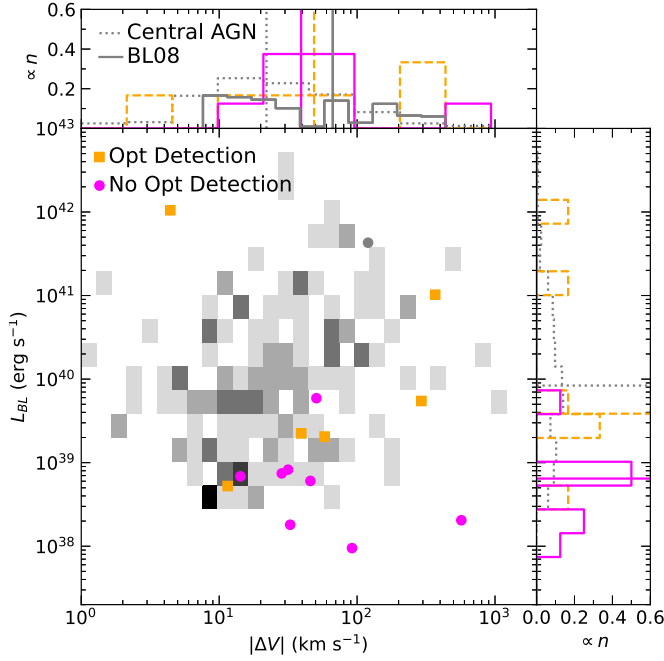


Figure 8. Broad emission line luminosity (L_{BL} ; total value from all spaxels) against the magnitude of the projected velocity offset relative to the host galaxy systemic velocity (ΔV ; flux-weighted average from all spaxels) for the central BLRs (linear-scale density map) and the subset of spatially offset BLRs with (orange squares) and without (magenta circles) optical image counterpart detections. The distributions of L_{BL} and ΔV are shown along the right and top axes, respectively, for the offset BLRs with (orange dashed) and without (magenta solid) image counterpart detections and for the central BLRs (gray dotted). The mean $|\Delta V|$ values of the spatially offset samples show a bias toward larger values relative to the central sample (by 78%). For comparison, the simulated distribution of recoiling MBH projected velocities from Blecha & Loeb (2008) (BL08) is also shown (solid gray line), and the offset BLR mean values are consistent with it to within 41%.

et al. 2015; Barrows et al. 2023). Indeed, when limiting our sample to the subset without stellar core detections, the median value of L_{BL}/M_* is ≥ 1.5 times larger than that of the central AGN sample.

6.2. Dual AGN and Extended Photo-ionization

A fraction of galaxy mergers are observed to host AGN in the nuclei of both galaxies (dual AGN; e.g., Komossa et al. 2003; Bianchi et al. 2008; Comerford et al. 2009; Piconcelli et al. 2010; Koss et al. 2012; Mazzarella et al. 2012; Comerford et al. 2015; Müller-Sánchez et al. 2015; Hou et al. 2022). The majority of AGN in such systems are buried under obscuring material that may also fuel the strongest stages of merger-driven MBH growth (e.g., Blecha et al. 2018). Optically-selected dual AGN in the nearby Universe, on the other hand, may represent sources in a relatively late stage of merger-driven AGN evolution after radiation pressure has removed ob-

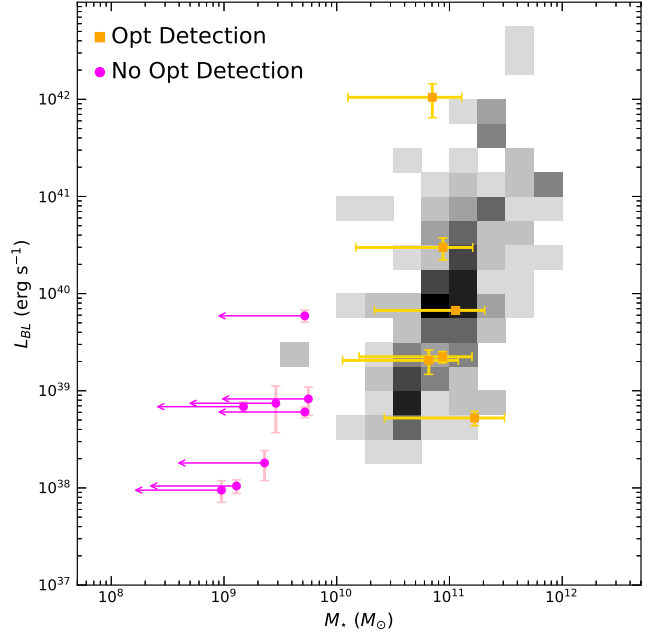


Figure 9. Broad emission line luminosities (L_{BL}) against the optical image counterpart stellar masses (M_* ; orange squares) or upper limits (for those without counterpart detections; magenta circles and left-pointing arrows). The density map shows the central AGN sample from this work. The subset without counterpart detections has relatively large L_{BL}/M_* ratios compared to central AGN, potentially due to merger-driven AGN enhancements and/or tidal stripping. Those without counterpart detections are also consistent with being ejected MBHs within faint hypercompact stellar systems.

scuring material (e.g., Hopkins et al. 2008; Hickox et al. 2009), thereby allowing tests of this connection.

Figure 7 shows that the $f_{A,Nuc}$ values are 74% higher for the offset broad line AGN with optical image counterparts relative to those without. Furthermore, the KS statistic and null hypothesis probability are 0.50 and 0.30, respectively (for both the [N II] and [S II] diagnostics) that they have similar $f_{A,Nuc}$ distributions. This observation may suggest that the offset broad line AGN in more massive galaxies have a higher probability of hosting dual AGN (i.e., a second optically-selected AGN in the host galaxy nucleus). This preference may be explained by their larger optical image counterpart stellar masses, since more massive galaxies are more likely to be in major mergers (e.g., Weigel et al. 2018), and major mergers may be more likely to host AGN (e.g., Somerville et al. 2001; Cox et al. 2008; Ellison et al. 2008). Hence, despite the lack of significant obscuring material, correlated triggering of optically-selected AGN in mergers may be efficient (e.g., Fu et al. 2018).

Alternatively, if no central AGN exists, these observations may be explained by the relatively higher L_{BL} val-

ues of the offset AGN with optical image counterparts (i.e., Figure 8) that may photo-ionize the ISM on spatially extended scales, including around the host galaxy nucleus. Indeed, 3 of the 6 likely infalling AGN have $f_{\text{A,BL}} > 0$ (between the [N II] and [S II] diagnostics combined) that suggest the AGN emission is strong enough to dominate the ionization potential over that of star formation. This possibility has implications for the nature of host galaxies with BPT indications of AGN, suggesting that not only can such narrow emission line ratios be produced by off-nuclear AGN, but they can also mimic the appearance of a nuclear BPT-selected AGN.

6.3. Surface Density of Recoiling AGN

Based on the survey footprint of MaNGA, the offset BLR sample without optical image counterparts from this work implies 5×10^{-3} recoiling AGN candidates per deg^2 with visible BLRs (an upper limit to the true surface density considering they are candidates). For comparison, assuming the random spin alignment model from Blecha et al. (2016), this is higher (by up to ~ 1 dex) than the predictions for photometric detections of recoiling AGN for all surveys considered in that work at $z < 0.15$ (approximate maximum redshift for the final MaNGA sample). Hence, since our measured surface density is an upper limit, it is consistent with these predictions and does not suggest highly efficient spin alignment in MBH binaries.

7. CONCLUSIONS

From the spatially-resolved spectroscopy of galaxies in the MaNGA survey, we have developed a sample of 14 candidate broad line AGN that are spatially offset from their host galaxy centroid by > 3 times the standard deviation of the source extent and by more than the MaNGA FWHM spatial resolution of $2''.5$ (14 and 1 from H α and H β detections, respectively, with an overlap of 1). The sample is based on the catalog of galaxies with broad emission lines (line widths of $\text{FWHM} > 1000 \text{ km s}^{-1}$) from Negus et al. (2024), which itself was derived from the 10,010 unique galaxies in the final MaNGA survey. This is the largest uniform sample of spectroscopically detected spatially offset broad line AGN candidates and the first such systematically generated sample from an IFS survey. The primary motivation for this project is to identify candidate recoiling or slingshot MBHs since such sources, if accreting as AGN, are expected to have unobscured BLRs that may have measurable nuclear offsets. Below we synthesize our interpretation of the nature of this sample and implications for merger-driven MBH growth and detection of recoiling AGN:

1. Regarding explanations that do not invoke offset AGN, we conclude the following: A) the probability of background or foreground chance projections is $< 2.7 \times 10^{-4}$; B) based on [O III] emission line models, no evidence is seen for narrow line outflows strong enough to mimic the presence of broad AGN components; C) while a supernova origin for the broad emission lines is expected to be rare, it can not be ruled out for any individual sources.
2. Based on the available SDSS imaging, optical counterparts are identified for 42% (6/14) of the sample. The stellar masses associated with the optical counterpart detections significantly exceed predictions for bound hypercompact stellar systems around recoiling MBHs. Therefore, they are likely to be infalling AGN in on-going galaxy mergers. The remaining 58% (8/14) only have upper limit masses on stellar counterparts and are therefore potentially consistent with being recoiling or slingshot MBHs.
3. Based on BPT diagnostics, the AGN-ionized narrow emission line signatures for the subset of the BLRs without optical image counterparts are 68% weaker than those for the subset with counterpart detections. An absence of narrow line AGN emission at the BLR position is consistent with predictions for the recoil or slingshot scenarios.
4. The projected velocity offsets (relative to the host galaxy systemic) of the BLR candidates that are spatially offset are 78% larger than for those in galaxy nuclei. This result suggests they may represent motion of the BLRs relative to the host galaxy, and they are also consistent (to within 41%) with predictions for observed recoiling AGN velocities. Furthermore, those without optical image counterparts have relatively lower luminosities (by a factor of 7), qualitatively consistent with predictions for recoiling AGN to accrete less efficiently.
5. In the scenario that the recoil/slingshot AGN candidates are actually infalling MBHs, those without optical counterpart detections have relatively large broad emission line luminosity to stellar counterpart mass ratios (> 1.5 times larger than for the central AGN). This result would be consistent with merger-driven triggering of broad line AGN being stronger in relatively low mass galaxies.
6. The AGN-ionized narrow emission line signatures in the host galaxy nuclei of the offset AGN candidates are 74% stronger for those with optical image

counterpart detections compared to those without counterparts. This may indicate they are more likely to host dual AGN, possibly since they are in more equal mass mergers with stronger tidal forces on each galaxy. Alternatively, since the off-set AGN candidates with optical image counterparts are more luminous, this result may indicate that they are photo-ionizing the ISM on spatially extended scales.

7. The surface density of ejected AGN candidates from this work is up to ~ 1 dex higher than predictions for recoiling AGN following random MBH spin alignments that can be found in photometric surveys. Since this sample can only provide an upper limit, this result is consistent with these predictions and hence does not suggest highly efficient MBH spin alignment in binaries.

In summary, the sample developed through this work contains 8 sources that are plausible candidates for ejected (recoil or slingshot) MBHs. Circumstantial evidence in favor of the ejected MBH scenario is in the form of BLRs with systematic velocity offsets from the host galaxy that are consistent with predictions for recoils, relatively low AGN luminosities, and relatively weak NLR AGN emission at the location of the BLRs. Those without evidence for NLR AGN emission in the host galaxy nucleus (J0946, J1124, J1508, J1604, and J1611) may be the strongest recoil candidates given the longer timescales for predicted recoil observability compared to those of AGN light echos. The remainder may be stronger candidates for slingshot MBHs. However, deeper imaging to search for faint stellar cores associated with the candidates is necessary for further consideration of the recoil or slingshot scenarios.

ACKNOWLEDGMENTS

We thank an anonymous reviewer for the detailed and thorough comments that have improved the manuscript quality. The authors thank Laura Blecha for insightful discussions that contributed to the interpretation of the results. J.M.C. and J.N. acknowledge support from NSF AST1714503 and NSF AST1847938. F.M.S. acknowledges support from NASA through awards 80NSSC19K1096 and 80NSSC23K1529. This project makes use of the MaNGA-Pipe3D dataproducts. We thank the IA-UNAM MaNGA team for creating this catalogue, and the Conacyt Project CB-285080 for supporting them. Funding for the Sloan Digital Sky Survey IV has been provided by the Alfred P. Sloan Foundation, the U.S. Department of Energy Office of Science,

and the Participating Institutions. SDSS-IV acknowledges support and resources from the Center for High Performance Computing at the University of Utah. The SDSS website is www.sdss4.org. SDSS-IV is managed by the Astrophysical Research Consortium for the Participating Institutions of the SDSS Collaboration including the Brazilian Participation Group, the Carnegie Institution for Science, Carnegie Mellon University, Center for Astrophysics | Harvard & Smithsonian, the Chilean Participation Group, the French Participation Group, Instituto de Astrofísica de Canarias, The Johns Hopkins University, Kavli Institute for the Physics and Mathematics of the Universe (IPMU) / University of Tokyo, the Korean Participation Group, Lawrence Berkeley National Laboratory, Leibniz Institut für Astrophysik Potsdam (AIP), Max-Planck-Institut für Astronomie (MPIA Heidelberg), Max-Planck-Institut für Astrophysik (MPA Garching), Max-Planck-Institut für Extraterrestrische Physik (MPE), National Astronomical Observatories of China, New Mexico State University, New York University, University of Notre Dame, Observatório Nacional / MCTI, The Ohio State University, Pennsylvania State University, Shanghai Astronomical Observatory, United Kingdom Participation Group, Universidad Nacional Autónoma de México, University of Arizona, University of Colorado Boulder, University of Oxford, University of Portsmouth, University of Utah, University of Virginia, University of Washington, University of Wisconsin, Vanderbilt University, and Yale University.

Facilities: Sloan

Software: Astropy⁴ (Astropy Collaboration et al. 2013, 2018, 2022), Marvin⁵ (Cherinka et al. 2019).

⁴ <http://www.astropy.org>

⁵ <https://dr16.sdss.org/marvin/>

APPENDIX

A. BEST-FITTING SPECTRAL MODELS

Figure 10 shows the spectral regions and best-fit models for which broad emission line components are detected (see Figure 3 for the others). The spectral models and broad emission line detections are from Negus et al. (2024). The blue excess peak in J133938.88+272416.5 resembles those of double-peaked broad line emitters and **has been fit with an additional Gaussian component**.

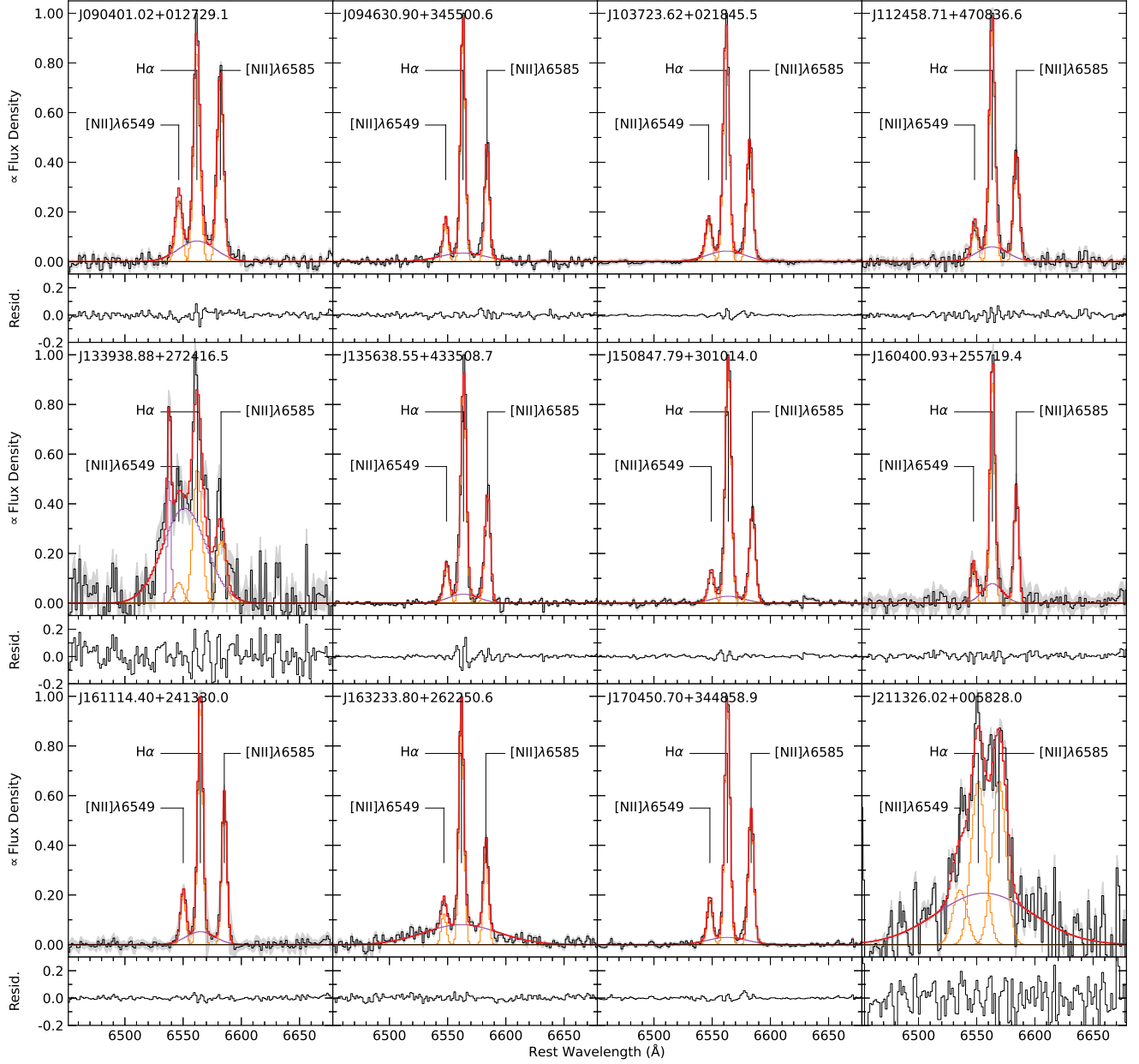


Figure 10. Same as Figure 3 but for the remainder of the sample (sorted by right ascension).

REFERENCES

- Astropy Collaboration, Robitaille, T. P., Tollerud, E. J., et al. 2013, *A&A*, 558, A33, doi: [10.1051/0004-6361/201322068](https://doi.org/10.1051/0004-6361/201322068)
- Astropy Collaboration, Price-Whelan, A. M., Sipőcz, B. M., et al. 2018, *AJ*, 156, 123, doi: [10.3847/1538-3881/aabc4f](https://doi.org/10.3847/1538-3881/aabc4f)
- Astropy Collaboration, Price-Whelan, A. M., Lim, P. L., et al. 2022, *ApJ*, 935, 167, doi: [10.3847/1538-4357/ac7c74](https://doi.org/10.3847/1538-4357/ac7c74)
- Barrows, R. S., Comerford, J. M., & Greene, J. E. 2018, *ApJ*, 869, 154, doi: [10.3847/1538-4357/aaedb6](https://doi.org/10.3847/1538-4357/aaedb6)
- Barrows, R. S., Comerford, J. M., Greene, J. E., & Pooley, D. 2016, *ApJ*, 829, 37, doi: [10.3847/0004-637X/829/1/37](https://doi.org/10.3847/0004-637X/829/1/37)
- . 2017, *ApJ*, 838, 129, doi: [10.3847/1538-4357/aa64d9](https://doi.org/10.3847/1538-4357/aa64d9)
- Barrows, R. S., Comerford, J. M., Stern, D., & Assef, R. J. 2023, *ApJ*, 951, 92, doi: [10.3847/1538-4357/acd2d3](https://doi.org/10.3847/1538-4357/acd2d3)
- Barrows, R. S., Lacy, C. H. S., Kennefick, D., Kennefick, J., & Seigar, M. S. 2011, *NewA*, 16, 122, doi: [10.1016/j.newast.2010.08.004](https://doi.org/10.1016/j.newast.2010.08.004)
- Barrows, R. S., Mezcuca, M., Comerford, J. M., & Stern, D. 2024, *ApJ*, 964, 187, doi: [10.3847/1538-4357/ad25fe](https://doi.org/10.3847/1538-4357/ad25fe)
- Bekenstein, J. D. 1973, *ApJ*, 183, 657, doi: [10.1086/152255](https://doi.org/10.1086/152255)
- Bertin, E., & Arnouts, S. 1996, *A&AS*, 117, 393
- Bianchi, S., Chiaberge, M., Piconcelli, E., Guainazzi, M., & Matt, G. 2008, *MNRAS*, 386, 105, doi: [10.1111/j.1365-2966.2008.13078.x](https://doi.org/10.1111/j.1365-2966.2008.13078.x)
- Blecha, L., Brisen, W., Burke-Spolaor, S., et al. 2019, *Astro2020: Decadal Survey on Astronomy and Astrophysics*, 2020, 318, doi: [10.48550/arXiv.1903.09301](https://doi.org/10.48550/arXiv.1903.09301)
- Blecha, L., Civano, F., Elvis, M., & Loeb, A. 2013, *MNRAS*, 428, 1341, doi: [10.1093/mnras/sts114](https://doi.org/10.1093/mnras/sts114)
- Blecha, L., Cox, T. J., Loeb, A., & Hernquist, L. 2011, *MNRAS*, 412, 2154, doi: [10.1111/j.1365-2966.2010.18042.x](https://doi.org/10.1111/j.1365-2966.2010.18042.x)
- Blecha, L., & Loeb, A. 2008, *MNRAS*, 390, 1311, doi: [10.1111/j.1365-2966.2008.13790.x](https://doi.org/10.1111/j.1365-2966.2008.13790.x)
- Blecha, L., Snyder, G. F., Satyapal, S., & Ellison, S. L. 2018, *MNRAS*, 478, 3056, doi: [10.1093/mnras/sty1274](https://doi.org/10.1093/mnras/sty1274)
- Blecha, L., Sijacki, D., Kelley, L. Z., et al. 2016, *MNRAS*, 456, 961, doi: [10.1093/mnras/stv2646](https://doi.org/10.1093/mnras/stv2646)
- Bogdanović, T., Eracleous, M., & Sigurdsson, S. 2009a, *NewA*, 53, 113, doi: [10.1016/j.newar.2009.09.005](https://doi.org/10.1016/j.newar.2009.09.005)
- . 2009b, *ApJ*, 697, 288, doi: [10.1088/0004-637X/697/1/288](https://doi.org/10.1088/0004-637X/697/1/288)
- Bonetti, M., Haardt, F., Sesana, A., & Barausse, E. 2016, *MNRAS*, 461, 4419, doi: [10.1093/mnras/stw1590](https://doi.org/10.1093/mnras/stw1590)
- . 2018, *MNRAS*, 477, 3910, doi: [10.1093/mnras/sty896](https://doi.org/10.1093/mnras/sty896)
- Bonning, E. W., Shields, G. A., & Salvander, S. 2007, *ApJL*, 666, L13, doi: [10.1086/521674](https://doi.org/10.1086/521674)
- Boroson, T. A., & Lauer, T. R. 2009, *Nature*, 458, 53, doi: [10.1038/nature07779](https://doi.org/10.1038/nature07779)
- Bundy, K., Bershad, M. A., Law, D. R., et al. 2015, *ApJ*, 798, 7, doi: [10.1088/0004-637X/798/1/7](https://doi.org/10.1088/0004-637X/798/1/7)
- Byrne-Mamahit, S., Hani, M., Ellison, S., Quai, S., & Patton, D. 2022, arXiv e-prints, arXiv:2212.07342, <https://arxiv.org/abs/2212.07342>
- Campanelli, M., Lousto, C., Zlochower, Y., & Merritt, D. 2007a, *ApJL*, 659, L5, doi: [10.1086/516712](https://doi.org/10.1086/516712)
- Campanelli, M., Lousto, C. O., Zlochower, Y., & Merritt, D. 2007b, *PhRvL*, 98, 231102, doi: [10.1103/PhysRevLett.98.231102](https://doi.org/10.1103/PhysRevLett.98.231102)
- Capelo, P. R., Volonteri, M., Dotti, M., et al. 2015, *MNRAS*, 447, 2123, doi: [10.1093/mnras/stu2500](https://doi.org/10.1093/mnras/stu2500)
- Centrella, J., Baker, J. G., Kelly, B. J., & van Meter, J. R. 2010, *Reviews of Modern Physics*, 82, 3069, doi: [10.1103/RevModPhys.82.3069](https://doi.org/10.1103/RevModPhys.82.3069)
- Cherinka, B., Andrews, B. H., Sánchez-Gallego, J., et al. 2019, *AJ*, 158, 74, doi: [10.3847/1538-3881/ab2634](https://doi.org/10.3847/1538-3881/ab2634)
- Chiaberge, M., Tremblay, G. R., Capetti, A., & Norman, C. 2018, *ApJ*, 861, 56, doi: [10.3847/1538-4357/aac48b](https://doi.org/10.3847/1538-4357/aac48b)
- Choksi, N., Behroozi, P., Volonteri, M., et al. 2017, *MNRAS*, 472, 1526, doi: [10.1093/mnras/stx2113](https://doi.org/10.1093/mnras/stx2113)
- Cisternas, M., Jahnke, K., Inskip, K. J., et al. 2011, *ApJ*, 726, 57, doi: [10.1088/0004-637X/726/2/57](https://doi.org/10.1088/0004-637X/726/2/57)
- Comerford, J. M., Barrows, R. S., Müller-Sánchez, F., et al. 2017, *ApJ*, 849, 102, doi: [10.3847/1538-4357/aa8e4b](https://doi.org/10.3847/1538-4357/aa8e4b)
- Comerford, J. M., Griffith, R. L., Gerke, B. F., et al. 2009, *ApJL*, 702, L82, doi: [10.1088/0004-637X/702/1/L82](https://doi.org/10.1088/0004-637X/702/1/L82)
- Comerford, J. M., Pooley, D., Barrows, R. S., et al. 2015, *ApJ*, 806, 219, doi: [10.1088/0004-637X/806/2/219](https://doi.org/10.1088/0004-637X/806/2/219)
- Comerford, J. M., Nevin, R., Negus, J., et al. 2024, *ApJ*, 963, 53, doi: [10.3847/1538-4357/ad1a15](https://doi.org/10.3847/1538-4357/ad1a15)
- Cox, T. J., Jonsson, P., Somerville, R. S., Primack, J. R., & Dekel, A. 2008, *MNRAS*, 384, 386, doi: [10.1111/j.1365-2966.2007.12730.x](https://doi.org/10.1111/j.1365-2966.2007.12730.x)
- Decarli, R., Dotti, M., Montuori, C., Liimets, T., & Ederoclite, A. 2010, *ApJL*, 720, L93, doi: [10.1088/2041-8205/720/1/L93](https://doi.org/10.1088/2041-8205/720/1/L93)
- Di Matteo, T., Springel, V., & Hernquist, L. 2005, *Nature*, 433, 604, doi: [10.1038/nature03335](https://doi.org/10.1038/nature03335)
- Dotti, M., Montuori, C., Decarli, R., et al. 2009, *MNRAS*, 398, L73, doi: [10.1111/j.1745-3933.2009.00714.x](https://doi.org/10.1111/j.1745-3933.2009.00714.x)
- Duncan, K., Conselice, C. J., Mundy, C., et al. 2019, *ApJ*, 876, 110, doi: [10.3847/1538-4357/ab148a](https://doi.org/10.3847/1538-4357/ab148a)
- Ellison, S. L., Patton, D. R., Simard, L., & McConnachie, A. W. 2008, *AJ*, 135, 1877, doi: [10.1088/0004-6256/135/5/1877](https://doi.org/10.1088/0004-6256/135/5/1877)

- Eracleous, M., Boroson, T. A., Halpern, J. P., & Liu, J. 2012, *ApJS*, 201, 23, doi: [10.1088/0067-0049/201/2/23](https://doi.org/10.1088/0067-0049/201/2/23)
- Eracleous, M., & Halpern, J. P. 2003, *ApJ*, 599, 886, doi: [10.1086/379540](https://doi.org/10.1086/379540)
- Eracleous, M., Livio, M., Halpern, J. P., & Storchi-Bergmann, T. 1995, *ApJ*, 438, 610, doi: [10.1086/175104](https://doi.org/10.1086/175104)
- Ferrarese, L., & Merritt, D. 2000, *ApJL*, 539, L9, doi: [10.1086/312838](https://doi.org/10.1086/312838)
- Fu, H., Steffen, J. L., Gross, A. C., et al. 2018, *ApJ*, 856, 93, doi: [10.3847/1538-4357/aab364](https://doi.org/10.3847/1538-4357/aab364)
- Gao, F., Wang, L., Pearson, W. J., et al. 2020, *A&A*, 637, A94, doi: [10.1051/0004-6361/201937178](https://doi.org/10.1051/0004-6361/201937178)
- Gaskell, C. M. 2009, *NewAR*, 53, 140, doi: [10.1016/j.newar.2009.09.006](https://doi.org/10.1016/j.newar.2009.09.006)
- Gebhardt, K., Bender, R., Bower, G., et al. 2000, *ApJ*, 539, L13, doi: [10.1086/312840](https://doi.org/10.1086/312840)
- Goulding, A. D., Greene, J. E., Bezanson, R., et al. 2018, *PASJ*, 70, S37, doi: [10.1093/pasj/psx135](https://doi.org/10.1093/pasj/psx135)
- Gualandris, A., & Merritt, D. 2008, *ApJ*, 678, 780, doi: [10.1086/586877](https://doi.org/10.1086/586877)
- Gültekin, K., Richstone, D. O., Gebhardt, K., et al. 2009, *ApJ*, 698, 198, doi: [10.1088/0004-637X/698/1/198](https://doi.org/10.1088/0004-637X/698/1/198)
- Hao, L., Strauss, M. A., Tremonti, C. A., et al. 2005, *AJ*, 129, 1783, doi: [10.1086/428485](https://doi.org/10.1086/428485)
- Hickox, R. C., Jones, C., Forman, W. R., et al. 2009, *ApJ*, 696, 891, doi: [10.1088/0004-637X/696/1/891](https://doi.org/10.1088/0004-637X/696/1/891)
- Hinshaw, G., Larson, D., Komatsu, E., et al. 2013, *The Astrophysical Journal Supplement Series*, 208, 19, doi: [10.1088/0067-0049/208/2/19](https://doi.org/10.1088/0067-0049/208/2/19)
- Hoffman, L., & Loeb, A. 2007, *MNRAS*, 377, 957, doi: [10.1111/j.1365-2966.2007.11694.x](https://doi.org/10.1111/j.1365-2966.2007.11694.x)
- Hopkins, P. F., Hernquist, L., Cox, T. J., & Kereš, D. 2008, *ApJS*, 175, 356, doi: [10.1086/524362](https://doi.org/10.1086/524362)
- Hou, M., Li, Z., Liu, X., et al. 2022, *arXiv e-prints*, arXiv:2212.06399. <https://arxiv.org/abs/2212.06399>
- Jadhav, Y., Robinson, A., Almeyda, T., Curran, R., & Marconi, A. 2021, *MNRAS*, 507, 484, doi: [10.1093/mnras/stab2176](https://doi.org/10.1093/mnras/stab2176)
- Kalfountzou, E., Santos Lleo, M., & Trichas, M. 2017, *ApJL*, 851, L15, doi: [10.3847/2041-8213/aa9b2d](https://doi.org/10.3847/2041-8213/aa9b2d)
- Keel, W. C., Maksym, W. P., Bennert, V. N., et al. 2015, *AJ*, 149, 155, doi: [10.1088/0004-6256/149/5/155](https://doi.org/10.1088/0004-6256/149/5/155)
- Kewley, L. J., Groves, B., Kauffmann, G., & Heckman, T. 2006, *MNRAS*, 372, 961, doi: [10.1111/j.1365-2966.2006.10859.x](https://doi.org/10.1111/j.1365-2966.2006.10859.x)
- Kocevski, D. D., Faber, S. M., Mozena, M., et al. 2012, *ApJ*, 744, 148, doi: [10.1088/0004-637X/744/2/148](https://doi.org/10.1088/0004-637X/744/2/148)
- Kokubo, M., Mitsuda, K., Morokuma, T., et al. 2019, *ApJ*, 872, 135, doi: [10.3847/1538-4357/aaff6b](https://doi.org/10.3847/1538-4357/aaff6b)
- Komossa, S. 2012, *Advances in Astronomy*, 2012, 364973, doi: [10.1155/2012/364973](https://doi.org/10.1155/2012/364973)
- Komossa, S., Burwitz, V., Hasinger, G., et al. 2003, *ApJL*, 582, L15, doi: [10.1086/346145](https://doi.org/10.1086/346145)
- Komossa, S., & Merritt, D. 2008a, *ApJL*, 689, L89, doi: [10.1086/595883](https://doi.org/10.1086/595883)
- . 2008b, *ApJL*, 683, L21, doi: [10.1086/591420](https://doi.org/10.1086/591420)
- Komossa, S., Xu, D., Zhou, H., Storchi-Bergmann, T., & Binette, L. 2008a, *ApJ*, 680, 926, doi: [10.1086/587932](https://doi.org/10.1086/587932)
- Komossa, S., Zhou, H., & Lu, H. 2008b, *ApJ*, 678, L81, doi: [10.1086/588656](https://doi.org/10.1086/588656)
- Koss, M., Mushotzky, R., Treister, E., et al. 2012, *ApJL*, 746, L22, doi: [10.1088/2041-8205/746/2/L22](https://doi.org/10.1088/2041-8205/746/2/L22)
- Koss, M., Blecha, L., Mushotzky, R., et al. 2014, *MNRAS*, 445, 515, doi: [10.1093/mnras/stu1673](https://doi.org/10.1093/mnras/stu1673)
- Kuncarayakti, H., Sollerman, J., Izzo, L., et al. 2023, *A&A*, 678, A209, doi: [10.1051/0004-6361/202346526](https://doi.org/10.1051/0004-6361/202346526)
- Lacerda, E. A. D., Sánchez, S. F., Mejía-Narváez, A., et al. 2022, *NewA*, 97, 101895, doi: [10.1016/j.newast.2022.101895](https://doi.org/10.1016/j.newast.2022.101895)
- LaMassa, S. M., Cales, S., Moran, E. C., et al. 2015, *ApJ*, 800, 144, doi: [10.1088/0004-637X/800/2/144](https://doi.org/10.1088/0004-637X/800/2/144)
- Law, D. R., Cherinka, B., Yan, R., et al. 2016, *AJ*, 152, 83, doi: [10.3847/0004-6256/152/4/83](https://doi.org/10.3847/0004-6256/152/4/83)
- Lena, D., Jonker, P. G., Rauer, J. P., Hernandez, S., & Kostrzewa-Rutkowska, Z. 2020, *MNRAS*, 495, 1771, doi: [10.1093/mnras/staa1174](https://doi.org/10.1093/mnras/staa1174)
- Li, S., Liu, F. K., Berczik, P., Chen, X., & Spurzem, R. 2012, *ApJ*, 748, 65, doi: [10.1088/0004-637X/748/1/65](https://doi.org/10.1088/0004-637X/748/1/65)
- Liu, H.-Y., Liu, W.-J., Dong, X.-B., et al. 2019, *ApJS*, 243, 21, doi: [10.3847/1538-4365/ab298b](https://doi.org/10.3847/1538-4365/ab298b)
- Lotz, J. M., Jonsson, P., Cox, T. J., et al. 2011, *ApJ*, 742, 103, doi: [10.1088/0004-637X/742/2/103](https://doi.org/10.1088/0004-637X/742/2/103)
- Lousto, C. O., & Zlochower, Y. 2011, *PhRvD*, 83, 024003, doi: [10.1103/PhysRevD.83.024003](https://doi.org/10.1103/PhysRevD.83.024003)
- Lyke, B. W., Higley, A. N., McLane, J. N., et al. 2020, *ApJS*, 250, 8, doi: [10.3847/1538-4365/aba623](https://doi.org/10.3847/1538-4365/aba623)
- Markakis, K., Dierkes, J., Eckart, A., et al. 2015, *A&A*, 580, A11, doi: [10.1051/0004-6361/201425077](https://doi.org/10.1051/0004-6361/201425077)
- Mazzarella, J. M., Iwasawa, K., Vavilkin, T., et al. 2012, *AJ*, 144, 125, doi: [10.1088/0004-6256/144/5/125](https://doi.org/10.1088/0004-6256/144/5/125)
- McAlpine, S., Harrison, C. M., Rosario, D. J., et al. 2020, *MNRAS*, 494, 5713, doi: [10.1093/mnras/staa1123](https://doi.org/10.1093/mnras/staa1123)
- Meena, B., Crenshaw, D. M., Schmitt, H. R., et al. 2021, *ApJ*, 916, 31, doi: [10.3847/1538-4357/ac0246](https://doi.org/10.3847/1538-4357/ac0246)
- Merritt, D., Schnittman, J. D., & Komossa, S. 2009, *ApJ*, 699, 1690, doi: [10.1088/0004-637X/699/2/1690](https://doi.org/10.1088/0004-637X/699/2/1690)
- Müller-Sánchez, F., Comerford, J. M., Nevin, R., et al. 2015, *ApJ*, 813, 103, doi: [10.1088/0004-637X/813/2/103](https://doi.org/10.1088/0004-637X/813/2/103)

- Negus, J., Comerford, J. M., & Müller Sánchez, F. 2024, *ApJ*, 971, 92, doi: [10.3847/1538-4357/ad4c68](https://doi.org/10.3847/1538-4357/ad4c68)
- Nevin, R., Blecha, L., Comerford, J., et al. 2023, *MNRAS*, 522, 1, doi: [10.1093/mnras/stad911](https://doi.org/10.1093/mnras/stad911)
- Oh, K., Yi, S. K., Schawinski, K., et al. 2015, *ApJS*, 219, 1, doi: [10.1088/0067-0049/219/1/1](https://doi.org/10.1088/0067-0049/219/1/1)
- Peng, C. Y., Ho, L. C., Impey, C. D., & Rix, H.-W. 2010, *AJ*, 139, 2097, doi: [10.1088/0004-6256/139/6/2097](https://doi.org/10.1088/0004-6256/139/6/2097)
- Peres, A. 1962, *Physical Review*, 128, 2471, doi: [10.1103/PhysRev.128.2471](https://doi.org/10.1103/PhysRev.128.2471)
- Piconcelli, E., Vignali, C., Bianchi, S., et al. 2010, *ApJL*, 722, L147, doi: [10.1088/2041-8205/722/2/L147](https://doi.org/10.1088/2041-8205/722/2/L147)
- Robinson, A., Young, S., Axon, D. J., Kharb, P., & Smith, J. E. 2010, *ApJL*, 717, L122, doi: [10.1088/2041-8205/717/2/L122](https://doi.org/10.1088/2041-8205/717/2/L122)
- Runnoe, J. C., Eracleous, M., Mathes, G., et al. 2015, *ApJS*, 221, 7, doi: [10.1088/0067-0049/221/1/7](https://doi.org/10.1088/0067-0049/221/1/7)
- Runnoe, J. C., Cales, S., Ruan, J. J., et al. 2016, *MNRAS*, 455, 1691, doi: [10.1093/mnras/stv2385](https://doi.org/10.1093/mnras/stv2385)
- Runnoe, J. C., Eracleous, M., Pennell, A., et al. 2017, *ArXiv e-prints*. <https://arxiv.org/abs/1702.05465>
- Sánchez, S. F., Barrera-Ballesteros, J. K., Lacerda, E., et al. 2022, *ApJS*, 262, 36, doi: [10.3847/1538-4365/ac7b8f](https://doi.org/10.3847/1538-4365/ac7b8f)
- Satyapal, S., Ellison, S. L., McAlpine, W., et al. 2014, *MNRAS*, 441, 1297, doi: [10.1093/mnras/stu650](https://doi.org/10.1093/mnras/stu650)
- Schawinski, K., Koss, M., Berney, S., & Sartori, L. F. 2015, *MNRAS*, 451, 2517, doi: [10.1093/mnras/stv1136](https://doi.org/10.1093/mnras/stv1136)
- Schneider, D. P., Richards, G. T., Hall, P. B., et al. 2010, *AJ*, 139, 2360, doi: [10.1088/0004-6256/139/6/2360](https://doi.org/10.1088/0004-6256/139/6/2360)
- Schnittman, J. D., & Buonanno, A. 2007, *ApJL*, 662, L63, doi: [10.1086/519309](https://doi.org/10.1086/519309)
- Shen, Y., Richards, G. T., Strauss, M. A., et al. 2011, *ApJS*, 194, 45, doi: [10.1088/0067-0049/194/2/45](https://doi.org/10.1088/0067-0049/194/2/45)
- Shields, G. A., Rosario, D. J., Smith, K. L., et al. 2009, *ApJ*, 707, 936, doi: [10.1088/0004-637X/707/2/936](https://doi.org/10.1088/0004-637X/707/2/936)
- Sijacki, D., Springel, V., & Haehnelt, M. G. 2011, *MNRAS*, 414, 3656, doi: [10.1111/j.1365-2966.2011.18666.x](https://doi.org/10.1111/j.1365-2966.2011.18666.x)
- Skipper, C. J., & Browne, I. W. A. 2018, *MNRAS*, 475, 5179, doi: [10.1093/mnras/sty114](https://doi.org/10.1093/mnras/sty114)
- Sofue, Y., & Rubin, V. 2001, *ARA&A*, 39, 137, doi: [10.1146/annurev.astro.39.1.137](https://doi.org/10.1146/annurev.astro.39.1.137)
- Somerville, R. S., Primack, J. R., & Faber, S. M. 2001, *MNRAS*, 320, 504, doi: [10.1046/j.1365-8711.2001.03975.x](https://doi.org/10.1046/j.1365-8711.2001.03975.x)
- Springel, V., Di Matteo, T., & Hernquist, L. 2005, *ApJL*, 620, L79, doi: [10.1086/428772](https://doi.org/10.1086/428772)
- Steffen, J. L., Fu, H., Brownstein, J. R., et al. 2022, *arXiv e-prints*, arXiv:2212.02677. <https://arxiv.org/abs/2212.02677>
- Steinborn, L. K., Dolag, K., Comerford, J. M., et al. 2016, *MNRAS*, 458, 1013, doi: [10.1093/mnras/stw316](https://doi.org/10.1093/mnras/stw316)
- Steinhardt, C. L., Schramm, M., Silverman, J. D., et al. 2012, *ApJ*, 759, 24, doi: [10.1088/0004-637X/759/1/24](https://doi.org/10.1088/0004-637X/759/1/24)
- Stemo, A., Comerford, J. M., Barrows, R. S., et al. 2021, *ApJ*, 923, 36, doi: [10.3847/1538-4357/ac0bbf](https://doi.org/10.3847/1538-4357/ac0bbf)
- Stern, J., & Laor, A. 2012, *MNRAS*, 423, 600, doi: [10.1111/j.1365-2966.2012.20901.x](https://doi.org/10.1111/j.1365-2966.2012.20901.x)
- Sulentic, J. W., Marziani, P., & Dultzin-Hacyan, D. 2000, *ARA&A*, 38, 521, doi: [10.1146/annurev.astro.38.1.521](https://doi.org/10.1146/annurev.astro.38.1.521)
- Tsai, C.-W., Jarrett, T. H., Stern, D., et al. 2013, *ApJ*, 779, 41, doi: [10.1088/0004-637X/779/1/41](https://doi.org/10.1088/0004-637X/779/1/41)
- Valenti, E., Zoccali, M., Mucciarelli, A., et al. 2018, *A&A*, 616, A83, doi: [10.1051/0004-6361/201832905](https://doi.org/10.1051/0004-6361/201832905)
- Villforth, C., Hamann, F., Rosario, D. J., et al. 2014, *MNRAS*, 439, 3342, doi: [10.1093/mnras/stu173](https://doi.org/10.1093/mnras/stu173)
- Volonteri, M. 2007, *ApJL*, 663, L5, doi: [10.1086/519525](https://doi.org/10.1086/519525)
- Volonteri, M., & Madau, P. 2008, *The Astrophysical Journal*, 687, L57
- Weigel, A. K., Schawinski, K., Treister, E., Trakhtenbrot, B., & Sanders, D. B. 2018, *MNRAS*, 476, 2308, doi: [10.1093/mnras/sty383](https://doi.org/10.1093/mnras/sty383)
- Weston, M. E., McIntosh, D. H., Brodwin, M., et al. 2017, *MNRAS*, 464, 3882, doi: [10.1093/mnras/stw2620](https://doi.org/10.1093/mnras/stw2620)
- Wylezalek, D., Flores, A. M., Zakamska, N. L., Greene, J. E., & Riffel, R. A. 2020, *MNRAS*, 492, 4680, doi: [10.1093/mnras/staa062](https://doi.org/10.1093/mnras/staa062)
- Wylezalek, D., Zakamska, N. L., Greene, J. E., et al. 2018, *MNRAS*, 474, 1499, doi: [10.1093/mnras/stx2784](https://doi.org/10.1093/mnras/stx2784)
- Yan, L., Quimby, R., Ofek, E., et al. 2015, *ApJ*, 814, 108, doi: [10.1088/0004-637X/814/2/108](https://doi.org/10.1088/0004-637X/814/2/108)
- Yu, Q., Lu, Y., Mohayaee, R., & Colin, J. 2011, *ApJ*, 738, 92, doi: [10.1088/0004-637X/738/1/92](https://doi.org/10.1088/0004-637X/738/1/92)
- Yuan, F.-T., Argudo-Fernández, M., Shen, S., et al. 2018, *A&A*, 613, A13, doi: [10.1051/0004-6361/201731865](https://doi.org/10.1051/0004-6361/201731865)